International Journal of Pharmaceutics 404 (2011) 271–280

Contents lists available at ScienceDirect

International Journal of Pharmaceutics

journal homepage: www.elsevier.com/locate/ijpharm

Pharmaceutical Nanotechnology

Effects of organic solvents on drug incorporation into polymeric carriers and morphological analyses of drug-incorporated polymeric micelles

Yoshiko Harada[a], Tatsuhiro Yamamoto[b], Masaru Sakai[c], Toshiharu Saiki[c,d], Kumi Kawano[e], Yoshie Maitani[e], Masayuki Yokoyama[b,f,*]

[a] Japan Science and Technology Agency, ERATO, Takahara Soft Interfaces Project, CE80, Kyushu University, 744 Motooka, Nishi-ku, Fukuoka 819-0395, Japan
[b] Yokoyama Nanomedical Project, Kanagawa Academy of Science and Technology, KSP East 404, 3-2-1 Sakado, Takatsu-ku, Kawasaki 213-0012, Japan
[c] Near-Field Optics Group, Kanagawa Academy of Science and Technology, KSP East-409, 3-2-1 Sakado, Takatsu-ku, Kawasaki 213-0012, Japan
[d] Department of Electronics and Electrical Engineering, Faculty of Science and Technology, Keio University, 3-14-1 Hiyoshi, Kohoku-ku, Yokohama-shi, Kanagawa-ken 223-8522, Japan
[e] Institute of Medicinal Chemistry, Hoshi University, 2-4-41 Ebara, Shinagawa-ku, Tokyo 142-8501, Japan
[f] Medical Engineering Laboratory, Research Center for Medical Science, Jikei University School of Medicine, 3-25-8, Nishi-shinbashi, Minato-ku, Tokyo 105-8461 Japan

ARTICLE INFO

Article history:
Received 20 August 2010
Received in revised form 21 October 2010
Accepted 11 November 2010
Available online 18 November 2010

Keywords:
Polymeric micelle
Camptothecin
Incorporation
Inner core
Targeting
Morphology

ABSTRACT

We incorporated an anticancer agent, camptothecin (CPT), into polymeric micelle carriers by using two different solvents (TFE and chloroform) in the solvent-evaporation drug incorporation process. We observed significant differences in the drug-incorporation behaviors, in the morphologies of the incorporated drug and the polymeric micelles, and in the pharmacokinetic behaviors between the two solvents' cases. In particular, the CPT-incorporated polymeric micelles prepared with TFE as the incorporation solvent exhibited more stable circulation in blood than those prepared with chloroform. This contrast indicates a novel technological perspective regarding the drug incorporation into polymeric micelle carriers. Morphological analyses of the inner core have revealed the presence of the directed alignment of the CPT molecules and CPT crystals in the micelle inner core. This is the first report of the morphologies of the drug incorporated into the polymeric micelle inner cores. We believe these analyses are very important for further pharmaceutical developments of polymeric micelle drug-carrier systems.

1. Introduction

Polymeric micelles have attracted much attention as a nano-sized drug carrier in drug delivery systems (DDS) (Yokoyama, 2005; Aliabadi and Lavasanifar, 2006; Yokoyama, 2007). Polymeric micelles are macromolecular assemblies that, formed from block copolymers or graft copolymers, have a spherical inner core and an outer shell (Tuzar and Kratochvil, 1976,). Most typically, polymeric micelle drug carrier systems form from an AB type of block copolymer possessing a hydrophobic block and a hydrophilic block (Bader et al., 1984; Yokoyama et al., 1989). Hydrophobic drugs are physically incorporated into the micelles' hydrophobic inner cores by means of hydrophobic interactions (Kwon et al., 1994a; Yokoyama et al., 1994; Molavi et al., 2008; Shin et al., 2009). Owing to their advantages such as very small size in a range of 10–100 nm and high structural stability, polymeric micelle carriers have been actively applied to drug targeting (Yokoyama et al., 1991; Yokoyama, 2005; Aliabadi and Lavasanifar, 2006). In particular, polymeric micelle systems have achieved successful tumor targeting (Kwon et al., 1994b; Yokoyama et al., 1999; Nishiyama et al., 2003; Kawano et al., 2006) through the enhanced permeability and retention (EPR) effect (Matsumura and Maeda, 1986; Maeda et al., 1992), which enables nano-sized carriers to deliver anti-cancer drugs selectively to solid tumor sites. Presently, five clinical trials are underway for tumor targeting with polymeric micelle systems (Matsumura et al., 2004; Hamaguchi et al., 2005; Koizumi et al., 2006; Hamaguchi et al., 2007; Nakajima et al., 2008a,b).

Among the several types of nano-sized carrier systems including liposomes, nano-spheres, antibodies, and water-soluble synthetic polymers, the polymeric micelle has exhibited strong advantages in applications to hydrophobic low-molecular-weight drugs owing to the micelle's large drug-loading capacity and the micelle's ability to maintain the water solubility of the given carrier system. Previous studies of polymeric micelle drug-carrier systems have indicated that the stable incorporation of drugs into the hydrophobic inner cores is essential for successful in vivo targeting (Yokoyama et al., 1999; Yokoyama, 2005). If the stability is low, the drug is very rapidly released (within a range of only several minutes) from the carrier, resulting in unsuccessful targeting. Kwon et al. reported that extremely low diffusion constant

* Corresponding author. Tel.: +81 3 3433 1111x2336; fax: +81 3 3459 6005.
E-mail address: masajun2093ryo@jikei.ac.jp (M. Yokoyama).

0378-5173/$ – see front matter © 2010 Elsevier B.V. All rights reserved.
doi:10.1016/j.ijpharm.2010.11.016

values in a 10^{-19} to 10^{-20} cm^2/s order were necessary for stable drug incorporation because the size of micelle inner cores is very small, being approximately 10 nm in diameter (Forrest et al., 2006a,b). Yokoyama et al. reported that a slight change in the chemical structures of inner-core-forming hydrophobic polymer chains had substantial effects on incorporation stability (Yokoyama et al., 2004; Watanabe et al., 2006; Yamamoto et al., 2007). However, little is known about key factors for stable incorporation. Furthermore, physico-chemical characterizations of the incorporated drug molecules have never been conducted even though these characterizations would no double be useful both for the elucidation and the achievement of incorporation stability. These characterizations may concern, for example, types of drug distribution (uniformly distributed or localized at specific sites such as a boundary with an outer shell), aggregation status (the dispersed individual drug molecules or the aggregation of drug molecules into a cluster), and drug molecules' polarity (randomly directed drug molecules or molecules aligned to a specific direction owing to intermolecular interactions). Researchers have reported that two successful polymeric micelle systems physically incorporated drug molecules possessing planar chemical structures, doxorubicin (Yokoyama et al., 1991, 1999) and camptothecin (CPT) (Watanabe et al., 2006; Yamamoto et al., 2007). Doxorubicin possesses a planar anthracycline ring, and CPT molecules have a planar five-membered-ring structure. Planar molecules can exhibit strong polarity if they are aligned in one direction through their intermolecular associations. Therefore, the polarity of incorporated drug molecules is a candidate for determining factors that underlie stable incorporation.

In this paper, we carry out the first physico-chemical examination of the incorporated drug molecules inside micelle inner cores by means of fluorescence spectroscopy and AFM. Furthermore, we evaluate effects that solvents used in drug-incorporation procedures can have on both the morphologies of inner cores and the morphologies of micelle structures. Then, we compare two polymeric micelle formulations that are different from each other only in the solvent used in the drug incorporation process, while the other factors, drug molecules and block copolymer structures, are the same between the two formulations. We observed a substantial difference in pharmacokinetic behaviors. This indicates that solvents can be an important factor in successful drug incorporation through the control of morphologies, whether in relation to incorporated drugs or polymeric micelles.

2. Materials and methods

2.1. Materials

(s)-(+)-Camptothecin and 1,1,1-trifluoro-2-propanol were purchased from Sigma-Aldrich (Tokyo branch, Japan) and were used as received. Reagent-grade solvents, chloroform, 2,2,2-trifluoroethanol (TFE), tetrahydrofuran (THF), dimethylsulfoxide (DMSO), N,N-dimethylformamide (DMF), N,N-dimethylacetamide (DMAc), 1,4-dioxane, 1,1,1,3,3,3-hexafluoro isopropanol were purchased from Wako Chemicals (Tokyo, Japan) and were used as received. Poly(ethylene glycol)-b-poly(aspartic acid-co-benzyl aspartate) (PEG-P(Asp(Bzl 74))) was synthesized as previously reported (Opanasopit et al., 2004; Yokoyama et al., 2004; Yamamoto et al., 2007), and its chemical structure is shown in Fig. 1. The average molecular weight of PEG was 5200 (n = 118 in Fig. 1), and the average number of Asp units (m) was 27. The current study converted 74% of the aspartic-acid units into benzyl-aspartate units through an esterification reaction of poly(ethylene glycol)-b-poly(aspartic acid). Our group has investigated variations of this type of block polymer by, for example, changing the percentage of benzyl aspartate units or using hydrophobic ester groups

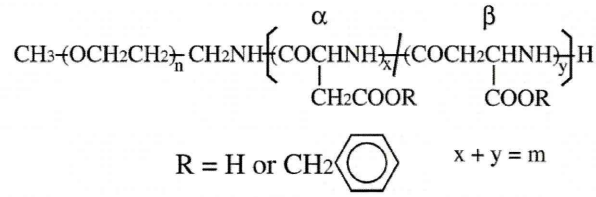

Fig. 1. Chemical structure of a block copolymer for micelle carriers.

other than benzyl ester, and so far PEG-P(Asp(Bzl 74) has worked well for our efforts to incorporate camptothecin into polymeric micelles (Yokoyama et al., 2004; Yamamoto et al., 2007) and to incorporate retinoids into polymeric micelles (Chansri et al., 2008; Okuda et al., 2008, 2009). The aspartate amide bond can be either α or β, and our group previously had reported that PEG-P(Asp(Bzl)) with all α aspartate amide bonds did not result in the formation of stable CPT-incorporated micelles. Therefore, in the current study, we used a polymer that has the aspartate amide bond with an α/β ratio of 1/3.

In some measurements, block copolymers possessing the same chain lengths and similar benzyl-esterification degrees (70% and 82%) were used.

2.2. Preparation of camptothecin-incorporated polymeric micelles

Camptothecin (CPT)-incorporated polymeric micelles were prepared through a solvent evaporation method (Yokoyama et al., 2004; Watanabe et al., 2006). In this method, 5 mg of PEG-P(Asp(Bzl 74)) and an appropriate amount of 1 mg/mL CPT solution (in TFE or chloroform) were mixed in a 9 mL glass vial, followed by evaporation of the solvent under a dry nitrogen-gas flow with stirring at 40–50 °C. After complete evaporation, a dried film was obtained. To this film was added 4 mL of water, and the mixture was sonicated with a probe type ultrasonication instrument (VCX-750 equipped with a 5 mm tapered micro tip, Sonics & Materials, Newtown, CT, USA). For removal of possible precipitates and large particles, the obtained solution was centrifuged at 10,000 rpm (12,000 × g) for 10 min by the use of a centrifuge Himac CR21G equipped with an R20A2 rotor (Hitachi Koki Co., Ltd., Tokyo, Japan) at 20 °C, and then was filtered through a 0.45 μm Millex-HV PVDF filter (Millipore Corp., Billerica, MA, USA), resulting in an aqueous solution of CPT-incorporated polymeric micelles. Polymeric micelles prepared by the use of TFE are denoted as "micelle A", and those prepared by the use of chloroform as "micelle B". A blank experiment was conducted in the absence of the block copolymer for estimating the amount of free CPT that would not be incorporated into polymeric micelles but that would be included in the solution. As the blank controls in which no polymer was used, CPT in a 1 mg/mL solution was added to an empty vial so that the total mass of CPT would be 0.5, 1.0, 2.0, or 5.0 mg, corresponding to 10, 20, 40, or 100 wt.% CPT with respect to polymers if they were present. The solvent was removed by evaporation, followed by an addition of water, sonication, centrifugation, and filtration according to the same approach as that adopted in the preparation of the CPT micelle solution. The concentration of CPT was measured with a UV–vis spectrometer. The procedure for UV–vis measurements is described in the UV–-vis spectroscopy Section 2.3.2.

2.3. Measurements

2.3.1. Dynamic light scattering (DLS)

Particle sizes of micelles were measured with a dynamic light scattering (DLS) instrument DLS-7000 (Otsuka Electronics, Tokyo,

Japan). The DLS samples were prepared by dilution of the micelle solutions with filtered Millipore water, while the polymer concentration was kept above the critical micelle concentration (CMC) reported in our previous paper (Yamamoto et al., 2007). The measurements were made at 25 °C, and scattering was observed at a 90° angle with respect to the incident beam. The Cumulant average particle size and particle size distribution from a non-negative least square method were determined by the use of software provided with the instrument. The DLS sample concentration was adjusted so that the scattering intensity would be within the measurable range, while the polymer concentration would be above its CMC.

2.3.2. UV–vis spectroscopy

The CPT concentrations of the micelle solutions were determined with a UV–vis spectrometer (Jasco V-550, JASCO Corp., Tokyo, Japan). The path length of the quartz cell was 1 cm. The scan range was 250–600 nm; the band width was set at 0.5 nm. CPT concentrations were calculated from an equation obtained from a calibration plot. Typically, a 150 μL sample aqueous solution, 150 μL water, and 2.7 mL DMSO were mixed to provide a 9:1 (vol./vol.) mixture of DMSO and water, and the peak top absorbance at 365 nm (A365) and the absorbance at 600 nm (A600) were recorded. The subtracted values (A365–A600) were used for the [CPT] determination. The CPT recovery in the drug-incorporation procedure was calculated through division of the micelle solution's "CPT amount" by the feed-added "CPT amount". When water was used in relation to the DMSO-water mixture as the solvent for UV–vis measurements, the dilution was 1/10 instead of 1/20.

We investigated the solubility of CPT in several organic solvents such as THF, DMF, and 1,4-dioxane, as well as in fluorinated solvents such as TFE and 1,1,1,3,3,3-hexafluoro isopropanol. CPT was dissolved in each solvent (up to 5 mg/mL), and absorbance at 600 nm was measured with a UV–vis spectrometer. We estimated the solubility of CPT in each solvent by measuring turbidity at 600 nm, because the CPT molecule has no absorption at 600 nm, and thus the absorbance recorded at this wavelength is caused by the light scattering of aggregated CPT.

2.3.3. Fluorescence spectroscopy

We measured polarization degrees of CPT molecules in the polymeric micelles by using a fluorescence-spectroscopy instrument (Jasco FP-6500, JASCO Corp., Tokyo, Japan) equipped with a polarization unit (JASCO Corp., Tokyo, Japan). Fluorescent spectra were recorded with excitation and emission at 351.5 nm and 433.0 nm, respectively. Band widths of excitation and emission were set at 10 nm and 3 nm, respectively. A fluorescence anisotropy (r) value was obtained by the formula $r = (I_{vv} - G \times I_{vh})/(I_{vv} + G \times I_{vh})$, where G is equivalent to I_{hv}/I_{hh}, where I_{vv} is equivalent to fluorescence intensity at vertical (excitation, Ex) and vertical (emission, Em) positions, where I_{vh} is equivalent to fluorescence intensity at vertical (Ex) and horizontal (Em) positions, where I_{hv} is equivalent to fluorescence intensity at horizontal (Ex) and vertical (Em) positions, and where I_{hh} is equivalent to fluorescence intensity at horizontal (Ex) and horizontal (Em) positions.

2.3.4. Polarized fluorescence microscopy

Polarized fluorescence microscopy, featuring a hand-made microscope, was carried out for a dried polymeric micelle sample on a quartz plate. An Ar-ion laser (351.1 nm; Innova 300, Coherent Inc., California, U.S.A.) with a polarization controller (SIGMA KOKI, Tokyo, Japan) was used for excitation, and a perpendicularly polarized component of the fluorescence signal was selectively observed with a supersensitive CCD camera (C4742-95ER, Hamamatsu Photonics, Shizuoka, Japan).

2.3.5. Atomic force microscopy (AFM)

For imaging by atomic force microscopy (AFM), micellar solutions were deposited on freshly cleaved mica, rinsed with water after a few minutes, and air (or nitrogen) dried; in this way, films were obtained. Height-contrast and phase-contrast images were obtained in air with an atomic force microscope MFP-3D (Asylum Research, Santa Barbara, CA, USA) in AC mode.

2.3.6. Determination of CPT concentrations in plasma

A CPT micelle solution in 0.9 wt.% NaCl was administered via the tail vein to male ddY mice (5 weeks old) at 2.5 mg CPT/kg. At 4 h after injection, blood was collected with a heparinized syringe, and the collected blood sample was centrifuged so that plasma could be obtained. The plasma was acidified with a 0.15 M phosphoric acid aqueous solution, and CPT was extracted with 4/1 (vol./vol.) chloroform/methanol. The extracted CPT was analyzed by the use of an HPLC system (LC-10AT, Shimadzu Corp., Kyoto, Japan) equipped with a Tosoh TSK-gel ODS-80Ts column (Tosoh, Corp., Tokyo, Japan), and a fluorescence detector set at $\lambda_{ex} = 369$ nm and $\lambda_{em} = 426$ nm. The mobile phase was a 23/77 vol./vol. mixture of acetonitrile/triethylamine acetate buffer (1.0% vol./vol., pH 5.5), and the flow rate of 1.0 mL/min was used.

2.3.7. Calculation of cohesion parameters

The partial cohesion parameters (δD, δP, and δH) for CPT and polymers were calculated from the molar volumes and the Hansen parameters listed in a reference (Hansen, C.M., 2007), and the total (Hildebrand) cohesion (solubility) parameter δt was obtained with the equation $\delta t = (\delta D^2 + \delta P^2 + \delta H^2)^{1/2}$. The parameters for the hydrophobic block, P(Asp(Bzl 74)), were calculated as molar-ratio-averages of the two repeating units Asp (26%) and Asp(Bzl) (74%).

3. Results

3.1. Preparation of CPT-incorporated polymeric micelles

We used block copolymer PEG-P(Asp(Bzl 74)) for the incorporation of camptothecin (CPT) into the polymeric micelle. Our method for the drug incorporation into the micelles proceeded in two steps: solvent evaporation and sonication. We will denote micelles prepared by evaporation of TFE as "micelle A", and those prepared by evaporation of chloroform as "micelle B". Among them, samples containing different amounts of CPT were prepared, and they will be represented by how much wt.% CPT/polymer was used in the feed, i.e., 10% CPT, 20% CPT, and so on. Except for the solvent used in the film preparation, all other process factors were identical between micelles A and B. We varied the CPT/polymer ratio between 5 and 100% by weight, by adding an appropriate volume of 1 mg/mL CPT solution. Therefore, the total volume of the solvent was different for each sample, depending on the amount of CPT required.

3.2. Solubility of CPT in various solvents

We evaluated solubility of CPT in several organic solvents. We present the results with TFE, chloroform, and DMSO in Fig. 2 and omit other solvents for presentation clarity. In chloroform, the measured absorbance was similar to that in THF or DMSO up to 1 mg/mL, but it took a sudden jump at this concentration and went out of scale for [CPT] > 1 mg/mL. The solubility of CPT in THF and 1,4-dioxane was also poor as these solvents also gave high absorbance at 600 nm for even [CPT] < 1 mg/mL, and CPT was practically insoluble at the higher concentrations. On the other hand, CPT was well dissolved in TFE, DMSO, DMF, and DMAc. CPT was moderately soluble in 1,1,1-trifluoro-2-propanol and 1,1,1,3,3,3-hexafluoro isopropanol but not as soluble as TFE. From these results we concluded that

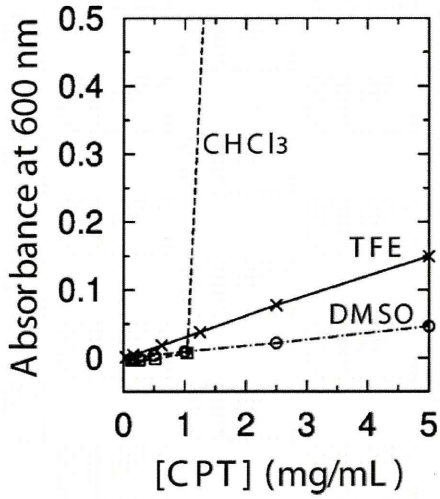

Fig. 2. Turbidity of CPT solutions in DMSO (○), TFE (×), and chloroform (□) as measured with a UV-VIS spectrometer.

the CPT solution used to prepare micelles should be in TFE or chloroform, and that [CPT] ≤1 mg/mL. One might consider the use of DMSO; however in our evaporation method, the solvent needs to be removed from the system. Therefore, solvents with a high boiling point are not preferred (b.p. DMSO = 189 °C, chloroform = 61 °C).

3.3. Characterization of CPT-incorporated micelles

3.3.1. Particle size determination by dynamic light scattering (DLS)

Fig. 3(a) shows the average Cumulant diameter of CPT micelles for various CPT amounts in the feed (5–100 wt.% with respect to polymers) as measured by DLS. The Cumulant average particle size ranged from ~80 to ~160 nm both for micelle A (prepared from TFE) and micelle B (prepared from CHCl3). The particle size of micelle B appeared to reach a limiting value of ~160 nm for a CPT/polymer weight ratio greater than 20%, whereas that of micelle A reached the first plateau between 20 and 40 wt.% CPT at ~110 nm, and then continued to increase to ~160 nm, reaching the second plateau between 40 and 60 wt.% CPT. Overall, the general tendency was that the particle size increased with the amount of CPT employed.

Fig. 4 shows the weight-weighted particle-size distribution of micelles prepared from 10 wt.% CPT/polymer as representative data. In Fig. 4(a), micelle A was observed to possess two peaks at 32 nm and 130 nm. Similarly, Fig. 4(b) corresponding to micelle B shows 2 peaks: one at 48 nm and the other at 168 nm, indicating that the aqueous micellar solutions contained two populations of particles. We assumed that the latter was a secondary association of micelles. In both of the micelle samples, the group of smaller particles constituted the majority (89% and 86% in weight for micelle A and micelle B, respectively) in the two populations.

3.3.2. CPT recovery in preparation of CPT-incorporated micelles

Fig. 3(b) shows CPT concentrations recovered in 4 mL of polymeric micelle aqueous solutions after the product was purified through centrifugation and filtration, plotted against the weight % of CPT/polymer in the feed. The same behaviors were observed between the average diameters shown in Fig. 3(a) and the CPT concentrations shown in Fig. 3(b) for both micelle A and micelle B. The CPT concentration in micelle B reached a plateau of ~20 wt.% CPT/polymer in the feed, where the maximum [CPT] value was ~80 μg/mL. This behavior was identical to the behavior of the Cumulant diameter shown in Fig. 3(a). Micelle A reached two

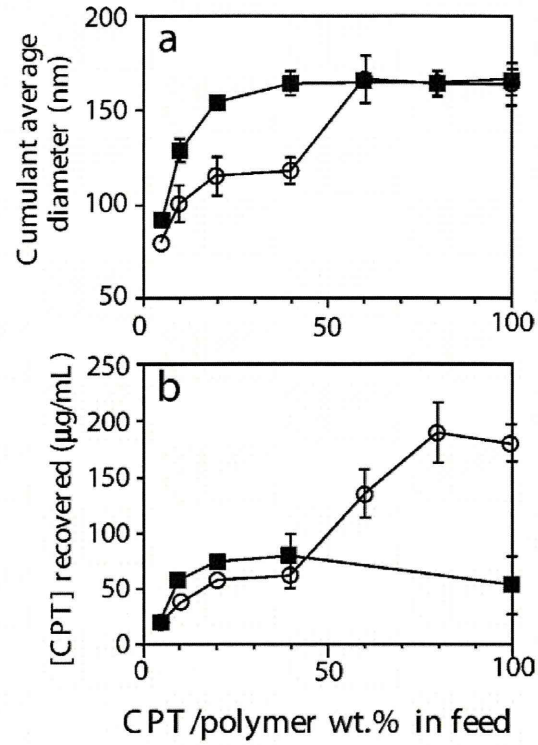

Fig. 3. CPT incorporation behaviors of polymeric micelles. (a) Cumulant average diameter of CPT micelles prepared with TFE(○, micelle A) or chloroform (■, micelle B). Data are shown in the average ± standard deviation of three measurements of the Cumulant average. (b) The CPT concentration recovered in an aqueous CPT micelle solution. Preparations of the micelles rested on TFE (○, micelle A) or chloroform (■, micelle B). Data are shown in the average ± standard deviation of three measurements.

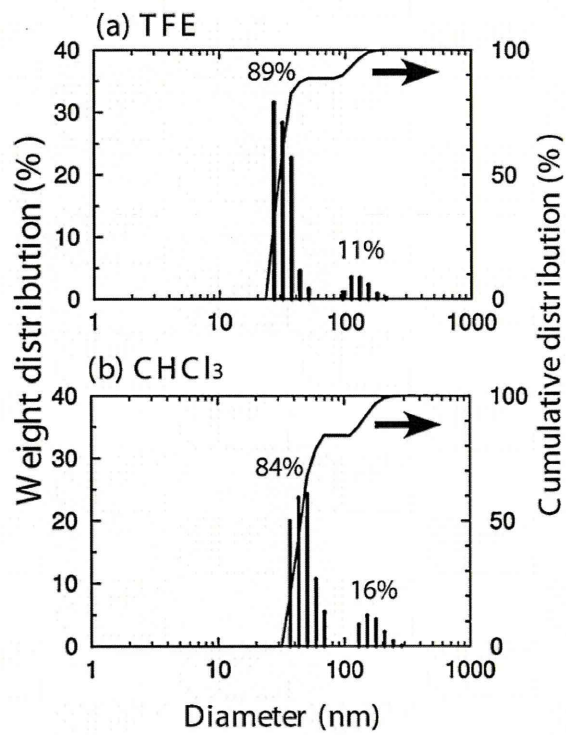

Fig. 4. Weight-weighted diameter distributions measured by dynamic light scattering for (a) micelle A (prepared from a solution in TFE) and (b) micelle B (prepared from a solution in chloroform). The CPT/polymer wt. ratio in the feed was 10% for the two cases. Values (%) shown in figures are weight proportions of the two peaks.

Table 1
CPT concentrations recovered after each step.

Solvent	CPT amounts in the feed[a]		[CPT] μg/mL after each step					
			Sonication→		Centrifugation→		Filtration	
TFE	0.5 mg	10 wt.%	120 ± 13	110	38 ± 5	31	5± 5	27
	2.0 mg	40 wt.%	470 ± 13	490	71 ±45	95	17 ±10	86
	5.0 mg	100 wt.%	I 1030 ±110	1100	66 ±10	170	27 ±12	160
CHCl3	0.5 mg	10 wt.%	89±23	140	8± 3	27	3± 0	27
	2.0 mg	40 wt.%	400 ± 44	560	18 ± 4	26	3± 1	25
	5.0 mg	100 wt.%	730 ± 24	1200	29 ±22	24	2± 1	23

Values at the left hand side are obtained without polymer and shown with the average ± S.D. ($n = 3$).Values at the right hand side are obtained with polymer ($n = 1$).
[a] CPT amounts are shown by weight for "without polymer" cases, and by CPT/polymer weight ratio in the feed for "with polymer" cases.

plateaus: the first one around 50 μg/mL at 20 wt.% CPT, and the second plateau around 190 μg/mL at 80 wt.% CPT. This was also the same behavior of the recovered CPT concentration shown in Fig. 3(a). In terms of efficiency (amount of CPT recovered/amount of CPT used), for micelle A, CPT was most efficiently recovered between levels of 5 and 10 wt.% CPT/polymer (~30% recovery), and efficiency of CPT recovery dropped to ~15% around 40 wt.% CPT, and then slightly improved in the 60–80 wt.% CPT range, and finally settled ~15% at 100 wt.% CPT/polymer. For micelle B, CPT recovery was highest at 10 wt.% CPT where ~45% of CPT used was recovered in the product, and then the efficiency of CPT recovery decreased steadily with the amount of CPT used. The lowest value in the range we examined in this study was only ~5% at 100 wt.% CPT. We treat the drop in the CPT recovery efficiency as a result of the precipitation of unincorporated CPT, as described below.

A series of experiments were conducted for estimation of the amount of unincorporated CPT. Concentrations of CPT in aqueous solutions were measured with a UV spectrometer after each step of the preparation procedure, namely, (1) the sonication step, (2) the centrifugation step, and (3) the filtration step. In these experiments, the procedure used for the CPT micelle preparation was carried out with and without the polymer. Table 1 summarizes results. The amount of CPT 0.5, 1.0, 2.0, or 5.0 mg in "without polymer" cases corresponded to 10, 20, 40, or 100% CPT/polymer ratios in "with polymer" cases. After the sonication step, considerably high amounts of CPT (ca. 60–100%) were recovered in both "with polymer" and "without polymer" cases, as revealed by the large values in Table 1's sonication columns. For "without polymer" cases, most of the recovered CPT seemed to be present as dispersion of small insoluble aggregates because the obtained solutions were turbid. Therefore, after the centrifugation step, the recovered CPT concentrations substantially dropped to 8–29 μg/mL for CHCl3 solvent cases and 38–71 μg/mL for TFE solvent cases owing to precipitation of the insoluble aggregates. In contrast, for "with polymer" cases, the recovered CPT amounts exhibited little change through the filtration step, while a considerable drop was observed in the "without polymer" cases after the filtration step possibly because of adsorption of the insoluble aggregates on a filter membrane

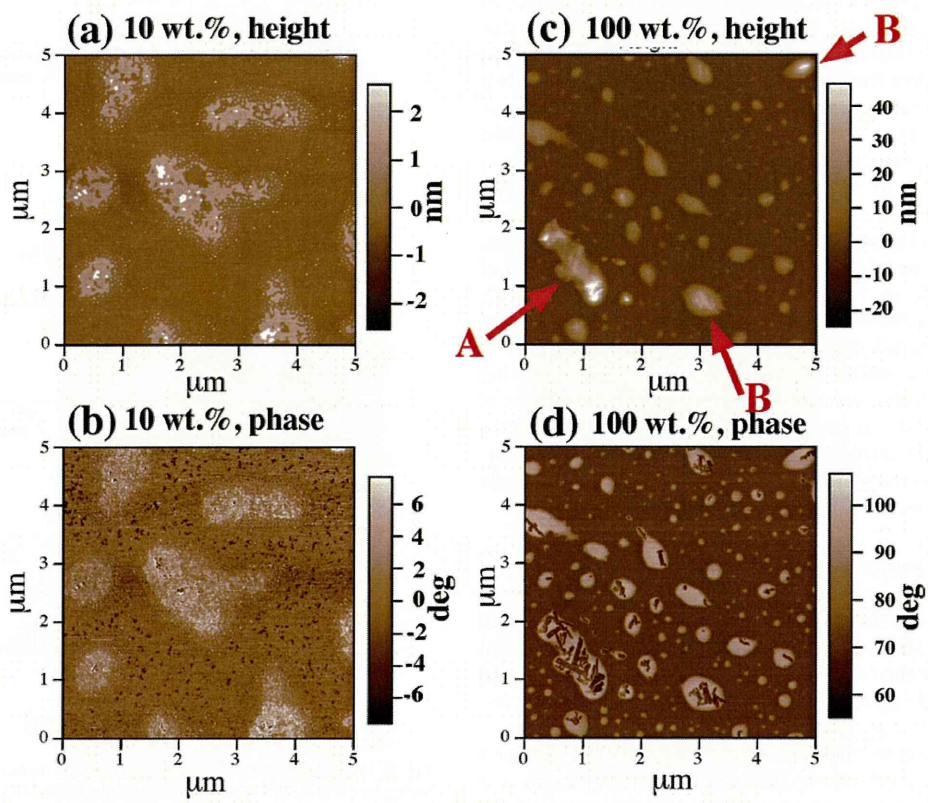

Fig. 5. AFM images of micelle A (prepared from a solution in TFE). The CPT/polymer wt.% in the feed was either 10% (a and b) or 100% (c and d). Images (a) and (c) are of height, while (b) and (d) concern phases.

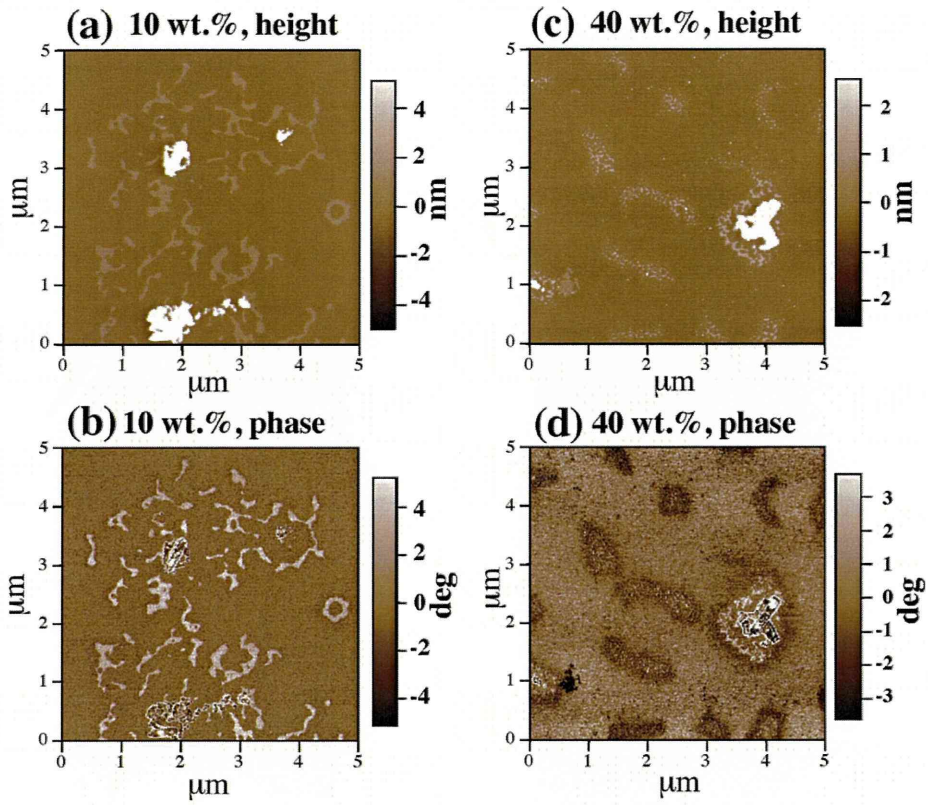

Fig. 6. AFM images of micelle B (prepared from a solution in chloroform). The CPT/polymer wt.% in the feed was either 10% (a and b) or 40% (c and d). Images (a) and (c) are of height, while (b) and (d) concern phases.

through hydrophobic interactions. These results indicate that most of the recovered CPT in the micelle solutions was incorporated into the polymeric micelles, and that low efficiency of the CPT incorporation at high CPT-polymer ratios resulted from the presence of large amounts of unincorporated CPT.

3.3.3. *Morphological observation of CPT-incorporated polymeric micelles by AFM*

AFM images of micelles are shown in Figs. 5 and 6. We obtained images by using dried films: aqueous micelle solutions were deposited on mica, and then the mica surfaces were rinsed with Millipore water for removal of excess sample, and finally dry nitrogen gas served to dry the surfaces. These dried films may not represent the real status of micelles in solution, but still provide useful topographical information on the samples.

A 5 μm × 5 μm scan of a film prepared from micelle A (10 wt.% CPT/polymer) shows patches of high contrast areas (Fig. 5, both height (a) and phase (b) images). The patches varied in size, but most of them occupied several hundred nm by several hundred nm to a few microns of area. The patches were relatively flat areas surrounded by small round-shaped islands less than 30 nm in diameter. Some islands were found also within patches; these spots were ~5–20 nm tall with respect to the surrounding flat area, whereas the flat area was <5 nm high with respect to the lowest part of the sample. In these images, we could not assign polymer locations or CPT locations.

Interesting images were observed in a film of micelle A prepared from a 100 wt.% CPT/polymer ratio (Fig. 5(c) and (d)). In the height image (Fig. 5(c)), round objects of various sizes ranging from ~10 nm to several hundred nm in diameter were present, along with larger elliptical objects. The cross-section of this image showed that the height difference between the dark area and the top of the largest island (pointed at with arrow A) was approximately 30 nm. In some other areas, smaller objects with brighter contrast were observed (pointed at with arrow B), indicating the existence of a different species from that of the round area. In the corresponding phase image (Fig. 5(d)), round objects in bright contrast were found at the same positions and in the same sizes as those in the height image, and in addition to these islands were observed rectangular objects of dark contrast on top of those islands. Judging from this image's phase intensity (gray scale bar on the side), the hardness of the rectangular areas was similar to that of the background (most likely bare mica, possible with some polymer coating), while the bright area was softer than the dark areas. We believe that the bright areas represent the polymer, and the dark rectangular areas represent the crystals of CPT. These crystal-like rods were ~0.1 μm × 1 μm or smaller, and were positioned on top of the polymer islands.

Fig. 6 shows AFM images of micelle B prepared from either 10 wt.% (a,b) CPT/polymer or 40 wt.% (c,d) CPT/polymer in the feed. Fig. 6(a) represents a height image obtained from micelle B prepared at a 10 wt.% CPT/polymer ratio. In this 5 μm × 5 μm image, the sample appears to have two distinct areas: string-like structures that are <5 nm tall with respect to the lowest point of the substrate, and areas of much higher contrast, ~50 nm tall with respect to the surrounding area. In the phase image, the latter structure seems to be a collection of smaller lumps whose contrast differs from the string-like structures. When the height contrast was optimized for these tall lumps (image not shown here), the rectangular rods were the same shape as that of the crystal-like structure in Fig. 5(d). Although these AFM measurements with the dried films may cause artifacts in the film preparation process, these results suggest two matters. One, CPT molecules formed crystals in a high CPR/polymer feed ratio. Second, empty (incorporating no

CPT molecules) polymeric micelles may be present more probably in a high CPR/polymer feed ratio.

Fig. 6(c) and (d) were obtained from micelle B prepared in CPT/polymer 40 wt.%. These images were similar to Fig. 5(a) and (b) obtained from micelle A prepared from 10 wt.% CPT/polymer in TFE. The patches that were <5 nm in height with respect to the lowest part of the substrate were ubiquitous and were similar to those of micelle A; however, in addition to these patches, rod-like structures of ~10–40 nm thickness compared to the surroundings were found. These rod-like objects were the same as those seen in Fig. 6(a) and (b). These results suggest that aggregation of CPT molecules occurred in micelle B in a more drastic manner than micelle A, and that the empty micelles were present in micelle B in a higher proportion than micelle A.

3.3.4. CPT in micelle solutions monitored by UV–vis spectroscopy

As described earlier, the amount of CPT contained in a micelle solution was determined in a mixture of DMSO and water (9:1, vol./vol.) by UV–vis spectroscopy. This mixed solvent dissolves both CPT and the hydrophobic block of the copolymer. Therefore, CPT molecules that were released from the polymeric micelles were measured in this mixed solvent. For such a measurement only the peak intensity was necessary, but we now turn to the spectrum itself measured in water to examine the environment that surrounds CPT. Fig. 7 shows UV spectra of aqueous CPT-incorporated micelle solutions prepared at various CPT/polymer ratios by the use of (a) TFE and (b) chloroform as a solvent in the micelle preparation. CPT micelle solutions were diluted to a 1/10 concentration in water, corresponding to a CPT concentration of ~2–20 μg/mL and corresponding to a polymer concentration of ~0.1 mg/mL that was much higher than polymer's critical micelle concentration (Yamamoto et al., 2007). The spectra were normalized at a peak intensity of 351.5 nm. There were two main peaks in the spectra, as shown in Fig. 7: 351.5 nm and 367.5 nm. The shoulder peak around 395 nm, which was prominent in 60–100 wt.% CPT/polymer in micelle A, suggests intermolecular association of CPT molecules. The same shoulder was also observed in micelle B for a CPT/polymer wt.% range of 20–100%, but to a lesser degree than micelle A. The hypochromic effect was also observed at 367.5 nm, where the peak intensity decreased for some of the samples, compared with that of 5% CPT/polymer samples. This also indicates the intermolecular association of CPTs' aromatic chromophores.

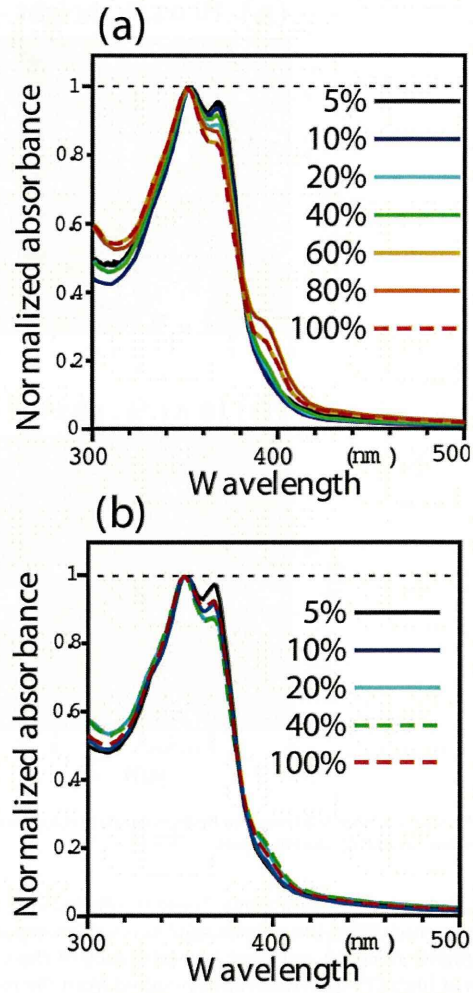

Fig. 7. Normalized UV spectra of CPT-incorporated micelles in aqueous solutions: (a) micelle A (prepared from a solution in TFE), and (b) micelle B (prepared from a solution in chloroform). The percentages shown in figures indicate the CPT/polymer wt.% in the feed.

3.3.5. Polarization degree of CPT molecules in the polymeric micelles

We evaluated the polarization degree of CPT molecules in the polymeric micelles by measuring the fluorescence anisotropy value (r). Fig. 8 shows the fluorescence anisotropy of CPT molecules in various CPT concentrations. The polarization degree reflects environments of incorporated CPT molecules. For polymeric micelle samples PEG-P(Asp(Bzl 70)) and PEG-P(Asp(Bzl 82)), the concentration of polymer was constant at 1.67 mg/mL, while CPT concentrations were varied through adjustments of CPT quantity used in the incorporation procedure into the micelles. Two influencing factors are present for the polarization degree; mobility/rigidity of environments where fluorescence molecules are present, and fluorescence extinction by the other fluorescence molecules. A greater polarization degree is observed for the fluorescence molecules in the more rigid (=less mobile) environments, while the polarization degree can change (raised or lowered) through the extinction by the other fluorescence molecules. Usually, the mobility/rigidity is the determining factor for the polarization degree of molecules incorporated in polymeric micelle inner cores, since it is obvious that the CPT molecules incorporated into the micelle inner core exist in a more rigid environment than the one where free CPT molecules dissolved in DMSO. (DMSO

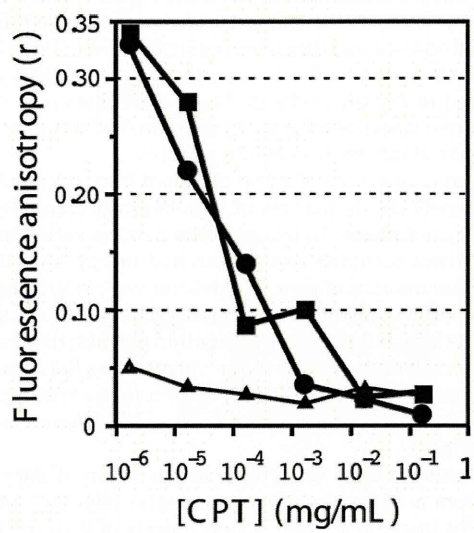

Fig. 8. Polarization degree of CPT fluorescence. CPT in polymeric micelles forming from PEG-P(Asp(Bzl 70)): ●, in polymeric micelles forming from PEG-P(Asp(Bzl 82)): ■, and CPT just dissolved in DMSO: ▲.

is a good solvent as proven in Fig. 2.) Unexpectedly, for these two polymeric micelle samples, the CPT polarization degrees were almost the same as or lower than the polarization degrees of free (unincorporated) CPT molecules dissolved in DMSO at high CPT concentrations of 1.7×10^{-1} and 1.7×10^{-2} mg/mL. This indicates that the fluorescence extinction was the determining factor in this CPT concentration range in a different manner from the usual polymeric micelle cases where the mobility/rigidity is the determining factor. In fact, the polarization degrees of the polymeric micelle samples were observed to become greater as the CPT concentration was lowered, while the polarization degrees were almost constant for the free CPT solution in DMSO in the whole measurement range. This tells two matters. One, the rigid micelle inner core environment was confirmed, as already reported with a dipyrene fluorescence probe (Yamamoto et al., 2007). Second, the polarization of CPT molecules can be detected, but only in much lower CPT concentration ranges than those used in actual formulations for in vitro and in vivo evaluations where a high CPT content (ca. 1–40 CPT wt. %) is preferably applied. Irrespective of this gap in the CPT concentration range, these results are the first information concerning drug molecule's incorporation status in the polymeric micelle inner core. By referring to this fact, we carried out the following polarized fluorescence microscopy measurements in this low CPT concentration range as described in the next section.

3.3.6. *Polarized fluorescence microscopy*

In order to detect the polarized fluorescence of CPT molecules, we carried out polarized fluorescence microscopy measurements on a quartz plate with a dried micelle sample having a low CPT/polymer ratio (0.001%, which corresponds to the micelle prepared at 1.7×10^{-5} mg/kg [CPT] in Fig. 8). At the emission side, the perpendicularly polarized component of the fluorescence signal was selectively observed with a supersensitive CCD camera, while at the excitation side an Ar-ion laser was applied with a polarization controller. As shown in Fig. 9, two bright spots were observed in this area, and fluorescence intensities of these two spots were found to change in accordance with the polarization controller angle. For spots A and B, both the brightest and darkest signals appeared with exactly 180° intervals. Therefore, it was revealed that this measurement detected the polarized fluorescence of the CPT molecules. This is the first direct visualization of the polarity of the drug molecules incorporated in polymeric micelles. Bright spots were not observed at higher CPT/polymer ratios (0.1%, 1%, and 10%, data not shown) owing to the florescence extinction observed in the polarized fluorescence spectra shown in Fig. 8. Therefore, this method could not reveal morphologies of the CPT molecules at the high CPT/polymer ratios that were used for in vitro and in vivo evaluations. The fluorescence extinction behaviors are dependent on excitation/emission characteristics of molecules; therefore, this method may be applied to drug molecules exhibiting prominent extinction behaviors. This polarized fluorescence technique can be a powerful and direct method to analyze morphologies of drug molecules in the micelle inner core.

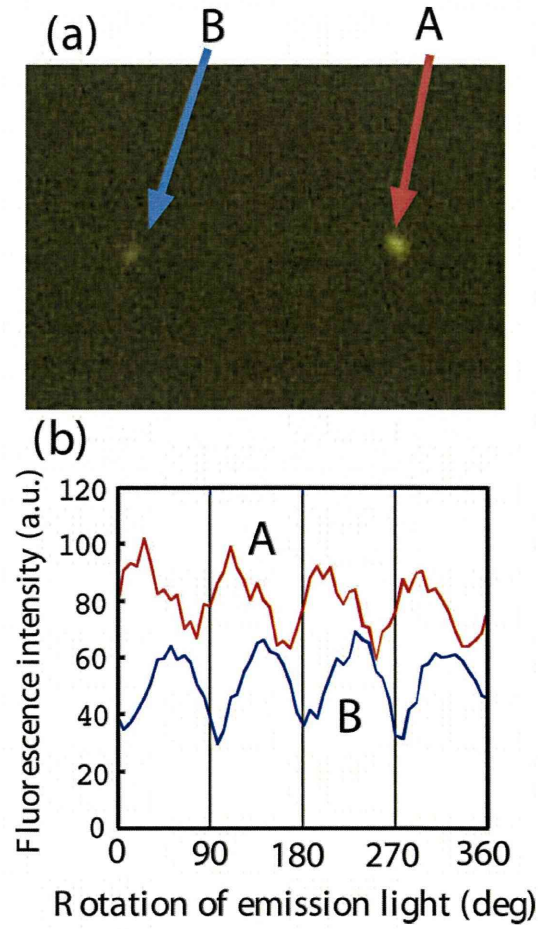

Fig. 9. Polarization fluorescence microscopic image (a) and its intensity change relative to the rotation of polarized emission light (b).

3.4. *Determination of CPT concentrations in plasma*

In Table 2, we summarize results of CPT concentrations in plasma at 4 h after intravenous injection of the CPT-incorporated polymeric micelles. We previously examined time course profiles in blood of [CPT] in polymeric micelles, and reported that CPT micelles prepared from PEG-P(Asp(Bzl 75)) exhibited the best in vivo stability value (9.3% dose) among similar polymers of various percentages of benzyl groups attached at the hydroxyl groups of P(Asp) (Watanabe et al., 2006). In this Table, we compare the values obtained from this previous report with our new results. In the previous method, CPT was incorporated by the use of chloroform as the evaporation solvent. We also observed that the CPT/polymer ratio did not affect so much (7.6 and 5.3% doses) the CPT concentrations in blood when we were using PEG-P(Asp(Bzl 57)), and

Table 2
CPT concentrations in blood 4 h after intravenous injection of polymeric micelles.

polymer	CPT/polymer wt. ratio in feed	solvent used for incorporation	CPT in blood (% dose)	reference
PEG-P(Asp(Bzl 74))	10%	TFE	27.3 ± 2.6	
PEG-P(Asp(Bzl 74))	5%	TFE	28.6 ± 0.5	
PEG-P(Asp(Bzl 75))	40%	Chloroform	9.3 ± 1.8	Watanabe et al., 2006
PEG-P(Asp(Bzl 57))	40%	Chloroform	7.6 ± 0.8	
PEG-P(Asp(Bzl 57))	10%	Chloroform	5.3 ± 0.6	

Table 3
Cohesion parameters of CPT, solvents, and an inner-core-forming polymer block.

	δD	δP	δH	δt
CPT	25.8	6.8	8.9	28.1
TFE	15.4	8.3	16.4	24.0
chloroform	17.8	3.1	5.7	18.9
DMSO	18.4	16.4	10.2	26.7
P(Asp) block	23.2	22.2	13.4	34.8
P(Asp (Bzl 74)) block	24.9	10.4	8.1	28.2

δD: dispersion solubility parameter.δP: Polar solubility parameter.δH: hydrogen bonding solubility parameter.δt: total (hildebrand) solubility parameter; $\delta t = (\delta D^2 + \delta P^2 + \delta H^2)^{1/2}$.Parameters are calculated according to methods and values of a reference (Hansen, 2007 Parameters of TFE, chloroform, and DMSO were taken from the reference. The units are: $(J\,cm^{-3})^{1/2}$.

that the CPT concentration did not exceed a 10% dose for the CPT-incorporated micelles prepared with chloroform. In contrast, with the polymeric micelles prepared from TFE, we obtained significantly higher CPT concentrations around the 28% dose. When we varied the CPT/polymer levels between 5% and 10%, no change in the CPT concentrations was observed. All these results indicate that the choice of organic solvent is an important key to obtaining the stable circulation of incorporated drugs in blood.

4. Discussion

In polymeric micelle research for drug delivery systems, most efforts have been made in carrier polymer design and preferable choice of the carrier polymer-drug combinations for the targetable carrier systems. The drug-incorporation process may be a very important step in preparing various polymeric micelle drug carrier systems; however, examinations of the topic are scarce. In this paper, we reported that the solvent used for the drug-incorporation process into polymeric micelles had substantial effects on drug-incorporation efficiency, micelle diameter, morphologies of the micelles and of the incorporated drug, and in vivo pharmacokinetic behavior of the incorporated drug. In particular, considerable prolongation of circulation in the bloodstream, which is essential for passive tumor targeting, was successfully obtained by the choice of an appropriate organic solvent used in the evaporation-"drug incorporation" method. As far as we know, this is the first indication of the solvent's importance for the prolongation of circulation in blood of polymeric micelle targeting systems.

When we used 2,2,2-trifluoroethanol (TFE) for the incorporation solvent, we obtained smaller average diameters of the micelles (in a drug/polymer ratio range from 5 wt.% to 40 wt.%) and more stable circulation in blood than the micelles did when prepared by the use of chloroform as the incorporation solvent. We think that the higher CPT solubility of TFE at CPT concentrations higher than 1 mg/mL is the reason for the preferable micelle formulation that exhibited the more stable circulation in blood than that of the chloroform case. Here, we conducted solubility and miscibility estimations by calculating solubility parameters. Table 3 lists the cohesion parameters of the materials: CPT, the solvents used in our experiment, and the hydrophobic block of the polymer. Theoretically, the smaller the difference between the δt of the drug and the solvent, the more soluble the drug is in the solvent (Huynh et al., 2008). If that is the case, the solubility of the three solvents' CPT is, from greater to smaller, DMSO > TFE > chloroform. This is in agreement with the results obtained from the turbidity experiment. Furthermore, the cohesion parameters of CPT are quite similar to those of the P(Asp(Bzl 74)) block of the polymer. This block copolymer PEG-P(Asp(Bzl 74) has been chosen from among several compositions and other hydrophobic moiety structures in terms of stable drug incorporation of CPT (Yokoyama et al., 2004; Yamamoto et al., 2007). Therefore, the calculated value agrees well with this fact. It is expected that the drug incorporation into the micelle inner core is of higher efficiency and is more stable when the drug is more miscible with the inner core-forming hydrophobic polymer block. However, more examinations with various combinations of the drug and the inner core-forming block are required for valuable applications of solubility-parameter calculations to reliable estimations of the optimized combination of a given drug and with a given carrier polymer.

We consider that the TFE's higher solubility of CPT efficiently inhibits large aggregates' formation of CPT molecules, resulting in higher CPT-incorporation yields and in the smaller micelle diameters than is the case with chloroform. AFM images in Fig. 6 indicate the presence of many empty micelles that do not contain CPT. This can be because large CPT aggregates formed aggressively during the solvent evaporation of chloroform, resulting in a large amount of unincorporated CPT aggregates.

As discussed above, this paper presents a novel methodology in polymeric micelle carrier systems for better formulations regarding the choice of an appropriate solvent in the evaporation drug-incorporation process. This is a very simple approach, but is no less important for being simple because the choice considerably changed pharmacokinetic behavior, as demonstrated in Table 3.

In addition to the importance of the solvent choice, this paper provided the first morphological information on incorporated drugs in polymeric micelles' inner cores. In general, morphological analyses of incorporated drugs are very difficult owing to the very small size of micelle inner cores (several nm). In this paper, we have shown the presence of the polarized CPT molecules in the inner cores by measuring fluorescence polarization spectra and microscopic images, as well as by measuring the formation of CPT crystals through AFM observations. We believe these morphological factors are very important for optimized drug incorporation into the polymeric micelle carriers although technical difficulties prevented us from identifying direct morphological evidence for stable CPT incorporation in the TFE case.

5. Conclusion

We observed substantial effects that solvents used in drug-incorporation processes can have on drug-incorporation behaviors, on the morphologies of both the incorporated drug and the polymeric micelles, and on pharmacokinetic behaviors. Simply through an appropriate choice of solvent, the circulation of an incorporated drug in blood was greatly improved for tumor targeting. Morphological analyses of the inner core revealed the directed alignment of the CPT molecules and CPT crystals in the micelle inner core at a low and high CPT/polymer ratio, respectively. These analyses are important for further developments of polymeric micelle drug-carrier systems.

Acknowledgements

This work was supported by the Ministry of Health, Labor, and Welfare of Japan and by both the JST CREST program and Grant-in-Aid of the Ministry of Education, Culture, Sports, Science, and Technology of Japan. Y. Harada, T. Yamamoto, and M. Yokoyama acknowledge the support from the Program for Promoting the Establishment of Strategic Research Centers, Special Coordination Funds for Promoting Science and Technology, and the Ministry of Education, Culture, Sports, Science and Technology of Japan. We thank Asylum Technology Co., LTD., Tokyo, Japan for providing access to an Atomic Force Microscopy MFP-3D.

References

Aliabadi, H.M., Lavasanifar, A., 2006. Polymeric micelles for drug delivery. Expert Opin. Drug Deliv. 3, 139–162.

Bader, H., Ringsdorf, H., Schmidt, B., 1984. Watersoluble polymers in medicine. Angew. Chem. 123/124, 457–485.

Chansri, N., Kawakami, S., Yokoyama, M., Yamamoto, T., Charoensit, P., Hashida, M., 2008. Anti-tumor effect of all-*trans* retinoic acid loaded polymeric micelles in solid tumor bearing mice. Pharm. Res. 25, 428–434.

Forrest, M.L., Won, C.Y., Malick, A.W., Kwon, G.S., 2006a. In vitro release of the mTOR inhibitor rapamycin from poly(ethylene glycol)-*b*-poly(ε-caprolactone) micelles. J. Contr. Rel. 110, 370–377.

Forrest, M.L., Zhao, A., Won, C.Y., Malick, A.W., Kwon, G.S., 2006b. Lipophilic prodrugs of Hsp90 inhibitor geldanamycin for nanoencapsulation in poly(ethylene glycol)-*b*-poly(ε-caprolactone) micelles. J. Contr. Rel. 116, 139–149.

Hamaguchi, T., Matsumura, Y., Suzuki, M., Shimizu, K., Goda, R., Nakamura, I., Nakatomi, I., Yokoyama, M., Kataoka, K., Kakizoe, T., NK105, 2005. A paclitaxel-incorporating micellar nanoparticle formulation, can extend in vivo antitumour activity and reduce the neurotoxicity of paclitaxel. Br. J. Cancer 92, 1240–1246.

Hamaguchi, T., Kato, K., Yasui, H., Morizane, C., Ikeda, M., Ueno, H., Muro, K., Yamada, Y., Okusaka, T., Shirao, K., Shimada, Y., Nakahama, H., Matsumura, Y., 2007. A phase I and pharmacokinetic study of NK105, a paclitaxel-incorporating micellar nanoparticle formulation. Br. J. Cancer 97, 170–176.

Huynh, L., Grant, J., Leroux, J.-P., Delmas, P., Allen, C., 2008. Predicting the solubility of the anti-cancer agent docetaxel in small molecule excipients using computational methods. Pharm. Res. 25, 147–157.

Kawano, K., Watanabe, M., Yamamoto, T., Yokoyama, M., Opanasopit, P., Okano, T., Maitani, Y., 2006. Enhanced antitumor effect of camptothecin loaded in long-circulating polymeric micelles. J. Contr. Rel. 112, 329–332.

Hansen, C.M., 2007. Hansen Solubility Parameters; A User's Handbook, second ed. CRC Press, Boca Raton.

Koizumi, F., Kitagawa, M., Negishi, T., Onda, T., Matsumoto, S., Hamaguchi, T., Matsumura, Y., 2006. Novel SN-38-incorporating polymeric micelles, NK012, eradicate vascular endothelial growth factor-secreting bulky tumors. Cancer Res. 66, 10048–10056.

Kwon, G.S., Naito, M., Kataoka, K., Yokoyama, M., Sakurai, Y., Okano, T., 1994a. Block copolymer micelles as vehicles for hydrophobic drugs. Colloids Surf. B: Biointerf. 2, 429–434.

Kwon, G.S., Suwa, S., Yokoyama, M., Okano, T., Sakurai, Y., Kataoka, K., 1994b. Enhanced tumor accumulation and prolonged circulation times of micelle-forming poly(ethylene oxide–aspartate) block copolymer–adriamycin conjugates. J. Contr. Rel. 29, 17–23.

Maeda, H., Seymour, L.W., Miyamoto, Y., 1992. Conjugates of anticancer agents and polymers: Advantages of macromolecular therapeutics in vivo. Bioconjugate Chem. 3, 351–361.

Matsumura, Y., Maeda, H., 1986. A new concept for macromolecular therapeutics in cancer chemotherapy: Mechanism of tumoritropic accumulation of proteins and the antitumor agent smancs. Cancer Res. 46, 6387–6392.

Matsumura, Y., Hamaguchi, T., Ura, T., Muro, K., Yamada, Y., Shimada, Y., Shirao, K., Okusaka, T., Ueno, H., Ikeda, M., Watanabe, N., 2004. Phase 1 clinical trial and pharmacokinetic evaluation of NK911, a micelle-encapsulated doxorubicin. Br. J. Cancer 91, 1775–1781.

Molavi, O., Ma, Z., Mahmud, A., Alshamsan, A., Samuel, J., Lai, R., Kwon, G.S., Lavasanifar, A., 2008. Polymeric micelles for the solubilization and delivery of STAT3 inhibitor cucurbitacins in solid tumors. Int. J. Pharm. 347, 118–127.

Nakajima, T.E., Yanagihara, K., Takigahira, M., Yasunaga, M., Kato, K., Hamaguchi, T., Yamada, Y., Shimada, Y., Mihara, K., Ochiya, T., Matsumura, Y., 2008a. Antitumor effect of SN-38-releasing polymeric micelles, NK012, on spontaneous peritoneal metastases from orthotopic gastric cancer in mice compared with irinotecan. Cancer Res. 68, 9318–9322.

Nakajima, T.E., Yasunaga, M., Kano, Y., Koizumi, F., Kato, K., Hamaguchi, T., Yamada, Y., Shirao, K., Shimada, Y., Matsumura, Y., 2008b. Synergistic antitumor activity of the novel SN-38-incorporating polymeric micelles, NK012, combined with 5-fluorouracil in a mouse model of colorectal cancer, as compared with that of irinotecan plus 5-fluorouracil. Int. J. Cancer 122, 2148–2153.

Nishiyama, N., Okazaki, S., Cabral, H., Miyamoto, M., Kato, Y., Sugiyama, Y., Nishio, K., Matsumura, Y., Kataoka, K., 2003. Novel cisplatin-incorporated polymeric micelles can eradicate solid tumors in mice. Cancer Res. 63, 8977–8983.

Okuda, T., Kawakami, S., Yokoyama, M., Yamamoto, T., Yamashita, F., Hashida, M., 2008. Block copolymer design for stable encapsulation of N-(4-hydroxyphenyl)retinamide into polymeric micelles in mice. Int. J. Pharm. 357, 318–322.

Okuda, T., Kawakami, S., Higuchi, Y., Satoh, T., Oka, Y., Yokoyama, M., Yamashita, F., Hashida, M., 2009. Enhanced in vivo antitumor efficacy of fenretinide encapsulated in polymeric micelles. Int. J. Pharm. 373, 100–106.

Opanasopit, P., Yokoyama, M., Watanabe, M., Kawano, K., Maitani, Y., Okano, T., 2004. Block copolymer design for camptothecin incorporation into polymeric micelles for passive tumor targeting. Pharm. Res. 21, 2003–2010.

Shin, H.C., Alani, A.W., Rao, D.A., Rockich, N.C., Kwon, G.S., 2009. Multi-drug loaded polymeric micelles for simultaneous delivery of poorly soluble anticancer drugs. J. Contr. Rel. 140, 294–300.

Tuzar, Z., Kratochvil, P., 1976. Block and graft copolymer micelles in solution. Adv. Colloid Interf. Sci. 6, 201–232.

Yamamoto, Y., Yokoyama, M., Opanasopit, P., Hayama, A., Kawano, K., Maitani, Y., 2007. What are determining factors for stable drug incorporation into polymeric micelle carriers? Consideration on physical and chemical characters of the micelle inner core. J. Contr. Rel. 123, 11–18.

Yokoyama, M., Inoue, S., Kataoka, K., Yui, N., Okano, T., Sakurai, Y., 1989. Molecular design for missile drug: Synthesis of adriamycin conjugated with IgG using poly(ethylene glycol)-poly(aspartic acid) block copolymer as intermediate carrier. Die Makromolekulare Chemie 190, 2041–2054.

Yokoyama, M., Okano, T., Sakurai, Y., Ekimoto, H., Shibazaki, C., Kataoka, K., 1991. Toxicity and antitumor activity against solid tumors of micelle-forming polymeric anticancer drug and its extremely long circulation in blood. Cancer Res. 51, 3229–3236.

Yokoyama, M., Okano, T., Sakurai, Y., Kataoka, K., 1994. Improved synthesis of adriamycin-conjugated poly(ethylene oxide)-poly(aspartic acid) block copolymer and formation of unimodal micellar structure with controlled amount of physically entrapped adriamycin. J. Contr. Rel. 32, 269–277.

Yokoyama, M., Okano, T., Sakurai, Y., Fukushima, S., Okamoto, K., Kataoka, K., 1999. Selective delivery of adriamycin to a solid tumor using a polymeric micelle carrier system. J. Drug Targeting 7, 171–186.

Yokoyama, M., Opanasopit, P., Maitani, Y., Kawano, K., Okano, T., 2004. Polymer design and incorporation method for polymeric micelle carrier system containing water-insoluble anti-cancer agent camptothecin. J. Drug Targeting 12, 373–384.

Yokoyama, M., 2005. Polymeric Micelles for the Targeting of Hydrophobic Drugs. In: Kwon, G.S. (Ed.), Drug and Pharmaceutical Sciences, Vol. 148, Polymeric Drug Delivery Systems. Taylor & Francis, Boca Raton, pp. 533–575.

Yokoyama, M., 2007. Polymeric micelles as nano-sized drug carrier systems. In: Domb, A.J., Tabata, Y., Kumar, M.N.V.R., Farber, S. (Eds.), Nanoparticles for Pharmaceutical Applications. American Scientific Publishers, Stevenson Ranch, pp. 63–72.

Watanabe, M., Kawano, K., Yokoyama, M., Opanasopit, P., Okano, T., Maitani, Y., 2006. Preparation of camptothecin-loaded polymeric micelles and evaluation of their incorporation and circulation stability. Int. J. Pharm. 308, 183–189.

International Journal of Pharmaceutics 404 (2011) 264–270

Contents lists available at ScienceDirect

International Journal of Pharmaceutics

journal homepage: www.elsevier.com/locate/ijpharm

Pharmaceutical Nanotechnology

Cell line-dependent internalization pathways determine DNA transfection efficiency of decaarginine-PEG-lipid

Tomohiro Izumisawa[a], Yoshiyuki Hattori[a,*], Masataka Date[a], Kazunori Toma[b], Yoshie Maitani[a]

[a] Institute of Medicinal Chemistry, Hoshi University, Shinagawa-ku, Tokyo 142-8501, Japan
[b] The Asahi Kasei Corp., Shizuoka, Japan

ARTICLE INFO

Article history:
Received 18 August 2010
Received in revised form 21 October 2010
Accepted 11 November 2010
Available online 18 November 2010

Keywords:
Cell-penetrating peptide
Oligoarginine
Nonviral gene delivery
Macropinocytosis
HeLa
KB
PC-3

ABSTRACT

Previously, we have reported that decaarginine-conjugated PEG-lipids (R10B) efficiently delivered plasmid DNA (pDNA) into human cervical carcinoma HeLa cells *via* macropinocytosis; however, the mechanism of cellular uptake by R10B was not evaluated in other cell lines. In this study, we investigated the internalization mechanism by R10B/pDNA complex (R10B-lipoplex) in human prostate tumor PC-3 and human nasopharyngeal tumor KB cells, and compared with that in HeLa cells. Although it was necessary for R10B-lipoplex to associate with heparan sulfate (HS) on the cell surface in all cell lines, the R10B-lipoplex was internalized primarily through clathrin-mediated endocytosis in PC-3 and KB cells, and macropinosytosis in HeLa cells. In HeLa cells, treatment with the R10B-lipoplex induced the formation of lamellipodia for macropinocytosis, but did not in KB and PC-3 cells. Furthermore, the highest transfection efficiency by R10B-lipoplex was observed in HeLa cells. These findings indicated that the R10B-lipoplex induced the formation of lamellipodia in HeLa cells after binding to HS on the cells and was then internalized by macropinocytosis, which could induce high gene expression because of escaping degradation in lysosomes. Cell physiology might be a critical factor in cellular internalization and efficient transfection by cell penetration peptide.

1. Introduction

Cell-penetrating peptides (CPPs), less than 30 amino acid residues in length, such as HIV-1 Tat fragments, are abundant in arginine residues and the number of arginine residues seems to be an important essential factor for cellular uptake (Futaki et al., 2001a; Kaplan et al., 2005; Mitchell et al., 2000; Wender et al., 2000; Zaro and Shen, 2003). CPPs were originally identified to have the ability to cross the plasma membrane (Derossi et al., 1994; Futaki et al., 2001b; Morris et al., 2001; Oehlke et al., 1998; Pooga et al., 1998; Vives et al., 1997); however, it has been recently reported that cellular uptake of CPPs was inhibited by the presence of endocytosis inhibitors (Drin et al., 2003; Fischer et al., 2004; Vives, 2003). In the process of cellular internalization by CPPs, the first step was attachment to the cell surface by electrostatic interaction with heparan sulfate proteoglycans (HSPGs). HSPGs have been reported to mediate gene transfer into cultured cells by CPPs, such as HIV-1 Tat (Console et al., 2003; Tyagi et al., 2001; Wadia et al., 2004) and oligoarginine (Fuchs and Raines, 2004; Kawamura et al., 2006; Kosuge et al., 2008; Suzuki et al., 2002). Nakase et al. have shown that the interaction of arginine-rich peptides with HSPGs activated intracellular signals to induce actin organization and promote macropinocytosis (Nakase et al., 2007). Macropinocytosis is one of the major endocytic pathways and accompanies membrane ruffling. Macropinosomes decrease their pH, but are not delivered to lysosomes, thus avoiding DNA degradation (Conner and Schmid, 2003), resulting in that transgene internalized by macropinocytosis could be effectively delivered to the nucleus and induce high gene expression.

Octaarginine peptide has been reported to be taken up by macropinocytosis in human cervical carcinoma (HeLa) and chinese hamster ovary (CHO) cells (Nakase et al., 2004, 2007), and T cells (Wadia et al., 2004). However, some researchers have reported that CPPs are taken up *via* clathrin-dependent or caveolae-dependent endocytosis even in the same cell lines (Richard et al., 2003, 2005; Potocky et al., 2003; Jones et al., 2005; Ferrari et al., 2003); Tat peptides were taken up by clathrin-mediated endocytosis in HeLa and CHO cells (Richard et al., 2003, 2005; Potocky et al., 2003), while Tat peptide and GST-Tat-GFP fusion peptide were taken up by caveolae-mediated endocytosis into HeLa and HeLa-derived cell line HL3T1 cells (Jones et al., 2005; Ferrari et al., 2003). In CPP-modified carriers, octaarginine-modified liposome was taken up *via* macropinocytosis into mouse fibroblast NIH3T3 cells (Khalil et al., 2006) and *via* both clathrin-mediated endocy-

* Corresponding author. Tel.: +81 3 5498 5097; fax: +81 3 5498 5097.
E-mail address: yhattori@hoshi.ac.jp (Y. Hattori).

0378-5173/$ – see front matter © 2010 Elsevier B.V. All rights reserved.
doi:10.1016/j.ijpharm.2010.11.017

tosis and macropinocytosis in Madin-Darby canine kidney MDCK cells (Fujiwara et al., 2010). Therefore, the exact cellular uptake mechanism of CPPs remains to be elucidated, because the cellular uptake mechanism of CPPs was dependent on the cell line.

Previously, we synthesized decaariginine-PEG-lipid (R10B), conjugating decaarginine and 3,5-bis(dodecyloxy)benzamide (BDB) with poly(ethylene glycol) (PEG) spacer (Furuhata et al., 2006a), and demonstrated that the cellular uptake mechanism of R10B/plasmid DNA complex (R10B-lipoplex) was mainly macropinocytosis in HeLa cells (Furuhata et al., 2008, 2009); however, we did not examine the uptake mechanisms of R10B-lipoplex in other cell lines. In this study, we selected three cell lines, HeLa, human prostate tumor PC-3 and human nasopharyngeal tumor KB cells, and investigated the mechanism of cellular uptake and transfection efficiency by R10B-lipoplex.

2. Materials and methods

2.1. Plasmid DNA

Plasmid DNA (pDNA) encoding the luciferase gene under the control of cytomegalovirus promoter (pCMV-luc) was constructed as previously described (Igarashi et al., 2006). A protein-free preparation of pCMV-luc was purified using the EndoFree Plasmid Max Kit (Qiagen, Hilden, Germany). Fluorescein isothiocianate (FITC) and rhodamine-labeling for pDNA were performed using the protocol of the Label IT TM-FITC labeling kit and Label IT TM-Rhodamine labeling kit (Mirus, Madison, WI, USA), respectively, as previously described (Furuhata et al., 2009).

2.2. Cell culture

HeLa cells were obtained from the European Collection of Cell Culture (Wiltshire, UK). KB and PC-3 cells were supplied by the Cell Resource Center for Biomedical Research, Tohoku University (Miyagi, Japan). HeLa cells were grown in Eagle's Minimum Essential Medium, and KB and PC-3 cells in RPMI-1640 medium, supplemented with 10% heat-inactivated fetal bovine serum (FBS) and kanamycin (100 μg/mL) at 37 °C in a 5% CO_2 humidified atmosphere.

2.3. Transfection

R10B was synthesized as previously reported (Furuhata et al., 2006a, 2006b). R10B solution was prepared at 5 mM by simply dispersing R10B in water. One microliter of micelle solution was added to 2 μg pDNA at a charge ratio (+/−) of 8.5/1 with gentle shaking and leaving at room temperature for 10–15 min. For transfection, the complex (R10B-lipoplex) was diluted with medium (1 mL) to 5 μM R10B and then gently added to the cells.

2.4. Luciferase assay

R10B-lipoplex of pCMV-luc was diluted with serum-free medium (5 μM at a concentration of R10B), and then gently added to the cells. After incubation for 3 h at 37 °C, the cells were added to culture medium (1 mL) containing 10% FBS and then incubated for another 21 h. Luciferase expression was measured as counts per sec (cps)/μg protein using the luciferase assay system (Pica gene; Toyo Ink Mfg. Co. Ltd., Tokyo, Japan) and BCA reagent (Pierce, Rockford, IL, USA) as previously reported (Furuhata et al., 2006a).

2.5. Measurement of the amount of heparan sulfate in the cells

To measure the amount of HS in the cell, the cells were lysed with sampling buffer containing 0.5% Triton X-100 in phosphate-buffered saline (PBS, pH 7.4). After they were centrifuged at 10,000 × *g* for 10 min, the protein concentration of the supernatant was quantitated with BCA protein assay reagent as described above. After 100 μg protein in the supernatants was digested by 1.8 mg/mL Actinase E (Kaken Pharmaceutical Co., Tokyo, Japan), the amount of HS was determined as μg HS/μg protein by a Heparan Sulfate ELISA Kit (Seikagaku Biobusiness Co., Tokyo, Japan).

2.6. Immunostaining for heparan sulfate

The cells were placed in a Lab-Tek Chamber slide glass (Nalge Nunc, Rochester, NY, USA), which was coated with human fibronectin on the surface as previously described (Hattori and Maitani, 2007). For immunostaining, the cells were fixed in 4% paraformaldehyde for 15 min at room temperature. After protein blocking with 5% goat serum for the cells, HS on the cell surface was identified using a rat anti-human heparan sulafate proteoglycan monoclonal antibody (Acris Antibodies GmbH, Herford, Germany) with Alexa 555-labeled goat anti-rat IgG (Invitrogen, Carlsbad, CA, USA) as the secondary antibody. The fluorescence was examined microscopically using an ECLIPSE TS100 microscope (Nikon, Tokyo, Japan).

2.7. Cellular uptake

To investigate the effect of HS on the cell surface on cellular uptake, the cells were digested with 1 unit/mL heparinase-III in medium at 37 °C for 30 min, and then transfected with the R10B-lipoplex of FITC-labeled pDNA in medium containing 10% FBS. To investigate the effect of HS in the medium on cellular uptake, the R10B-lipoplex was incubated with the medium containing 20 μg/mL heparin (Sigma Chemical Co.) for 15 min, and then incubated with the cells for 1 h. For investigation of the cellular uptake mechanism by endocytosis inhibitors, the cells were treated with medium containing 400 mM sucrose, 50 μM 5-(*N*-Ethyl-*N*-isopropyl) amiloride (EIPA; Sigma Chemical Co.) or 5 μg/mL filipin (Sigma Chemical Co.) for 30 min. After treatment, the cells were transfected with the R10B-lipoplex for 1 h in the presence of each inhibitor. After incubation, the amount of FITC-labeled pDNA in the cells was determined by examining fluorescence intensity on a FACSCalibur flow cytometer (Becton Dickinson, San Jose, CA, USA) as previously described (Furuhata et al., 2006a, 2006b).

2.8. Confocal laser scanning microscopy

For observation of lamellipodia-like formations, the cells were incubated with R10B-lipoplex or 400 ng/mL EGF (Wako Pure Chemical Industries, Ltd., Osaka, Japan) for 5 min. After incubation, the cells were fixed with 4% formaldehyde and then cellular F-actin was stained with phalloidin-TRITC (Sigma Chemical Co.) after treatment with 0.1% Triton X-100 in PBS. For investigation of the cellular uptake mechanism, the cells were co-incubated for 3 h with R10B/rhodamine-labeled pDNA and 0.5 mg/mL Oregon green 488-labeled dextran (70 kDa, anionic, lysine fixable, Invitrogen). After incubation, the cells were fixed with 4% formaldehyde.

Examinations were performed with a LSM5 EXCITER confocal laser scanning microscope (Carl Zeiss, Thornwood, NY) as previously described (Furuhata et al., 2009). For phalloidin-TRITC and rhodamine-labeled pDNA, maximal excitation was performed with a 543-nm internal He–Ne laser, and fluorescence emission was observed with an LP560. Oregon green 488-labeled dextran was imaged using an argon laser at 488 nm excitation, and fluorescence emission was observed with a filter, BP505-530.

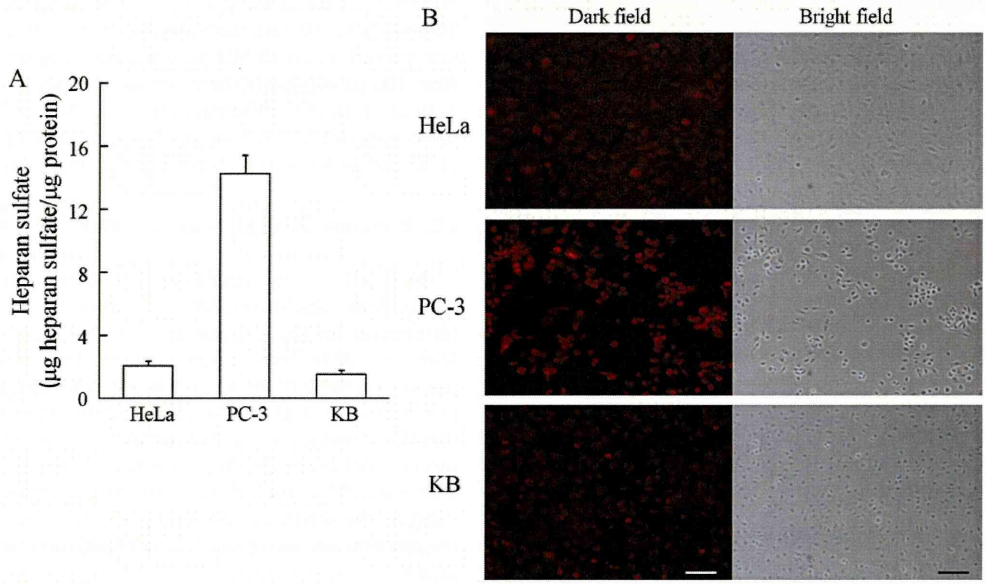

Fig. 1. Assessment of HS in HeLa, PC-3 and KB cells by ELISA (A) and immunostaining (B). In A, the amounts of HS were measured as μg HS/μg protein by the Heparan Sulfate ELISA-kit and BCA reagent. Each bar represents the mean ± S.D. of three experiments. In B, red indicates localization of heparan sulfate on the cell surface. Scale bar = 100 μm.

2.9. Statistical analysis

Significant differences in the mean values were evaluated by Student's unpaired *t*-test. A *p*-value of 0.05 or less was considered significant.

3. Results

3.1. Assessment of heparan sulfate amount in various cells

In the process of cellular internalization by CPPs, the first step was attachment to the cell surface by electrostatic interaction with HSPGs, which are transmembrane proteins conjugated to negatively charged sulfated glycan chains (heparan sulfate, HS); therefore, we first evaluated the amount of HS in three cell lines by ELISA and immunostaining (Fig. 1). The amounts of HS in homogeneous cell lysate of HeLa, PC-3 and KB cells by ELISA were 2.1 ± 0.2, 14.8 ± 1.3 and 1.6 ± 0.3 μg HS/μg protein, respectively (Fig. 1A). In immunostaining by anti-HS antibody, the presence of HS on the cell surface was strongly observed in PC-3 cells, and moderately in HeLa and KB cells (Fig. 1B), corresponding to the results by ELISA (Fig. 1A). From these findings, PC-3 cells had the highest amount of HS on the cell surface among the cell lines.

3.2. Effects of HS on cellular uptake

To investigate the effect of HS on cellular uptake by R10B-lipoplex, the cells were digested with heparinase-III before transfection. The digestion of HS significantly decreased the cellular amount of pDNA after transfection by the R10B-lipoplex to about 60% (Fig. 2). Heparin is closely related with heparan sulfate. The addition of heparin to the medium completely inhibited cellular uptake of the R10B lipoplex (Fig. 2). These results suggested that cell surface-expressed HSPGs played an important role in the cellular association with R10B-lipoplex.

3.3. Cellular uptake mechanism of R10B-lipoplex

To determine the uptake mechanism by R10B-lipoplex in three cell lines, we examined the effect of endocytosis inhibitors on the cellular uptake of R10B-lipoplex. EIPA is an inhibitor of macropinocytosis through the interaction with Na^+/H^+ exchanger, filipin of caveolae-mediated endocytosis through cholesterol depletion, and sucrose of clathrin-mediated endocytosis. EIPA strongly inhibited cellular uptake by the R10B-lipoplex in HeLa cells and weakly in KB cells (Fig. 3A); in contrast, sucrose strongly inhibited in PC-3 and KB cells (Fig. 3B and C), suggesting that the cellular uptake mechanism of the R10B-lipoplex in KB was mainly clathrin-mediated endocytosis and partly macropinocytosis, that in PC-3 cells was clathrin-mediated endocytosis and that in HeLa was macropinocytosis. Furthermore, to confirm the cellular uptake by macropinocytosis in HeLa cells, we observed the co-localization of R10B/rhodamine-labeled pDNA with Oregon green 488-labeled dextran, a marker of macropinocytosis. In HeLa cells, pDNA by transfection with R10B was co-localized with dextran (Fig. 4A), but not in PC-3 and KB cells (Fig. 4B and C), suggesting that the cellular uptake mechanism of R10B-lipoplex was macropinocytosis in

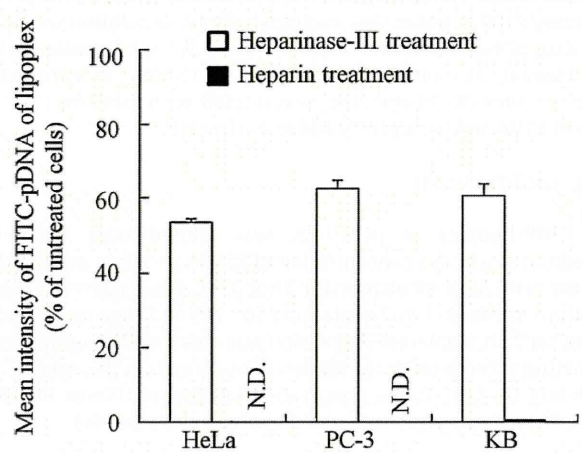

Fig. 2. Effects of HSPGs on cellular uptake of FITC-labeled pDNA by R10B-lipoplex. R10B-lipoplex was transfected into the cells for 1 h after treatment of the cells with heparinase-III (1 unit/mL) for 30 min (white bar) or after incubation of the R10B-lipoplex with heparin (20 μg/mL) for 15 min (black bar). Each bar represents the mean ± S.D. of three experiments.

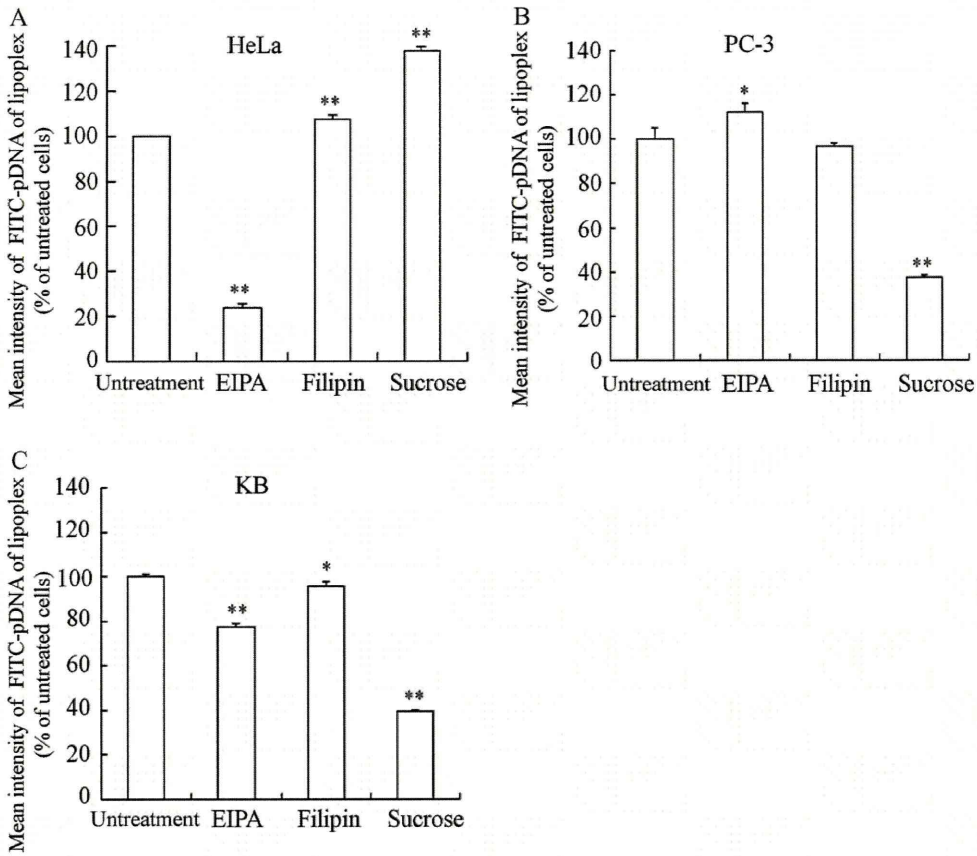

Fig. 3. Effect of endocytosis inhibitors on the cellular uptake of R10B-lipoplex in HeLa (A), PC-3 (B) and KB cells (C). The R10B-lipoplex of FITC-labeled pDNA was transfected into the cells after treatment with 50 μM EIPA, 5 μg/mL filipin or 400 mM sucrose for 30 min. Each bar represents the mean ± S.D. of three experiments. $^{*}P < 0.05$, $^{**}P < 0.01$, compared with untreated cells.

HeLa cells. The cellular uptake mechanism was not dependent on the amount of HS.

3.4. Induction of actin organization by R10B-lipoplex

Macropinocytosis accompanied the organization of F-actin and EGF induced the organization of F-actin, including lamellipodia-like formations (Nakase et al., 2004). To investigate why R10B-lipoplex was internalized by macropinocytosis in HeLa cells, we observed actin organization in the cells after treatment with R10B-lipoplex by confocal laser scanning microscopy (Fig. 5). EGF was used as a positive control for the induction of lamellipodia-like formations (Nakase et al., 2007). In R10B-lipoplex treatment, the induction of lamellipodia-like formations was observed in HeLa cells but not in PC-3 and KB cells. In contrast, the apparent organization of F-actin after the treatment with EGF was observed in all cells. These results suggested that R10B-lipoplex treatment could induce lamellipodia-like formations *via* the organization of F-actin only for HeLa cells.

3.5. Gene expression by R10B lipoplexes

Finally, we evaluated the transfection efficiency by R10B-lipoplex in the cells by assaying luciferase activity. Transfection activity by R10B-lipoplex was the highest in HeLa cells among the cell lines (Fig. 6). The transfection activity for HeLa cells was about 45-fold and 2500-fold higher than for PC-3 and KB cells, respectively. Although the amount of HS on the cell surface was highest in PC-3 cells (Fig. 1), the transfection activity in PC-3 cells was lower than in HeLa cells (Fig. 6).

4. Discussion

In this report, we investigated the cellular uptake mechanism and transfection activity by R10B-lipoplex in three cell lines, HeLa, PC-3 and KB cells. In the process of cellular internalization by CPPs, the first step was attachment to the cell surface by electrostatic interaction with HSPGs. The cellular uptake of R10B-lipoplex was inhibited in all the cell lines by heparinase-III treatment with the cells or heparin pretreatment with R10B-lipoplex (Fig. 2). Although the amount of HS was highest in PC-3 cells among the cell lines (Fig. 1), it was not correlated with the cellular uptake and transfection efficiency by R10B (Fig. 6). From these findings, HS was necessary for cellular association with R10B-lipoplex, but cellular uptake by R10B-lipoplex was independent of the amount of HS on the cell surface.

In effective transfection, elucidating the mechanism of R10B-lipoplex is a prerequisite to understanding and improving transfection. To investigate the cellular uptake mechanism of R10B-lipoplex, we examined the effect of endocytosis inhibitors on the cellular uptake of R10B-lipoplex. In HeLa cells, cellular association with the lipoplex decreased by EIPA, but did not decrease by sucrose (Fig. 3A); in contrast, in PC-3 and KB cells, it was mainly decreased by sucrose (Fig. 3B and C). These findings suggested that the internalization of R10B-lipoplex occurred mainly through macropinocytosis in HeLa cells, and clathrin-mediated endocytosis in PC-3 and KB cells. It has previously been reported that complex size can affect the mechanism of internalization, with clathrin-mediated endocytosis limited to particles under 200 nm, caveolae-mediated endocytosis for particles between 200 and

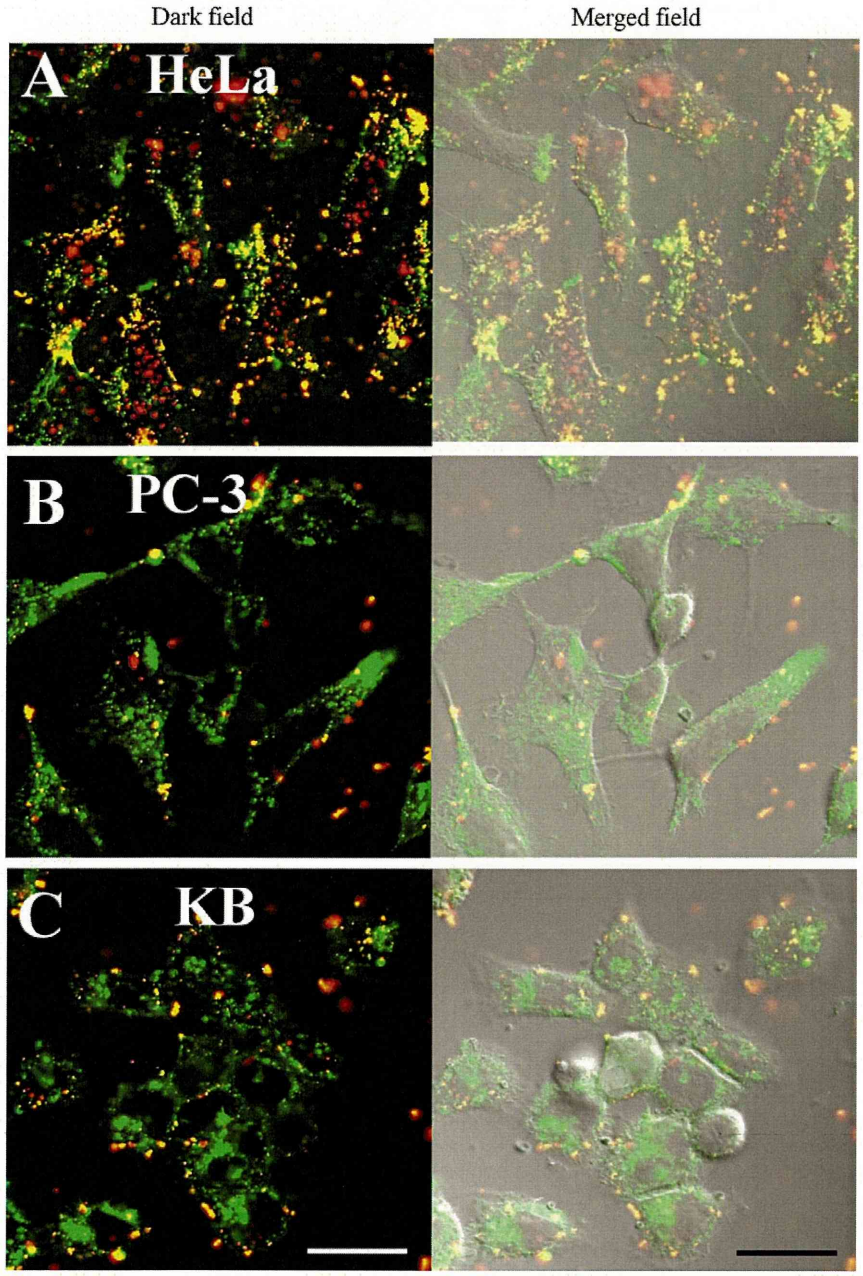

Fig. 4. Localization of R10B-lipoplex in cells by confocal microscopy. The cells were co-incubated with R10B/rhodamine-labeled pDNA and oregon green-labeled dextran for 3 h. Red shows the localization of pDNA and green that of dextran. Yellow indicates the co-localization of pDNA with dextran. Scale bar = 20 μm.

500 nm, and macropinocytosis for particles over 1 μm (Conner and Schmid, 2003; Medina-Kauwe et al., 2005; Rejman et al., 2004); however, the different pathways observed in our study cannot be explained by size, since all the cells were treated with similar-sized R10B-lipoplex (about 250 nm in medium, 0.28 in polydispersity index). It has been reported that the arginate-chitosan nanoparticle/pDNA complex was internalized through the clathrin-dependent pathway in 293T and COS7 cells, but through the caveolin-mediated pathway in CHO cells (Douglas et al., 2008). Moreover, CPPs have been reported to be taken up *via* macropinocytosis (Nakase et al., 2007), clathrin-dependent (Richard et al., 2003, 2005; Potocky et al., 2003) and caveolae-dependent endocytosis in HeLa and CHO cells (Jones et al., 2005; Ferrari et al., 2003). Although the exact cellular uptake mechanism of R10B-lipoplex remains to be elucidated, the cellular uptake mechanism of the lipoplex might be dependent on the cell line.

Macropinocytosis involves an actin-driven membrane protrusion (Conner and Schmid, 2003; Grimmer et al., 2002). Treatment with R10B-lipoplex induced actin-driven membrane ruffling in HeLa cells, but did not induce in PC-3 and KB cells (Fig. 5). It has been reported that the interaction of arginine-rich peptides with membrane-associated proteoglycans quickly activated the intracellular signals of Rac1 proteins and induced actin organization and lamellipodia following by macropinocytosis (Nakase et al., 2007; Schlunck et al., 2004; Nobes and Hall, 1995). It is not clear why R10B-lioplex could not induce lamellipodia in PC-3 and KB cells, but treatment with R10B-lipoplex might activate Rac1 protein in HeLa cells after binding to the cell surface but remain inactive in PC-3

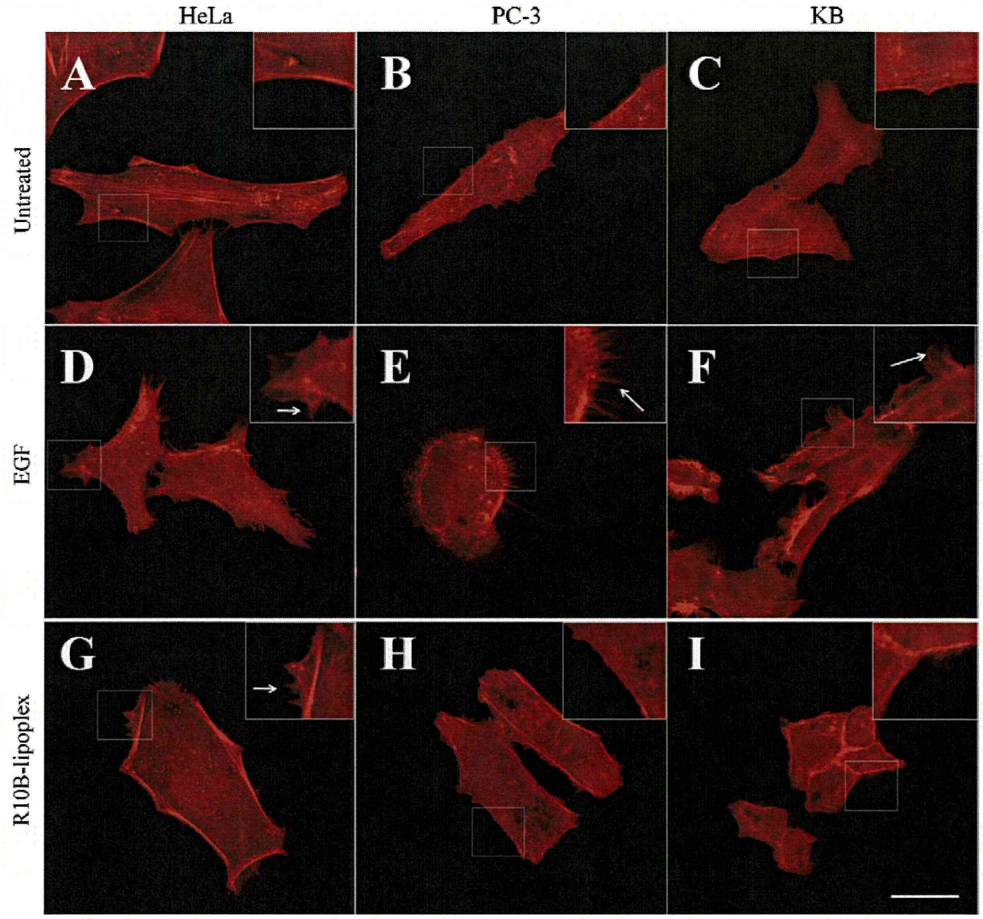

Fig. 5. Observation of lamellipodia formation by treatment with EGF (D–F) and R10B-lipoplex (G–I) in HeLa (A, D and G), PC-3 (B, E and H) and KB (C, F and I) cells. The cells were treated with 400 ng/mL EGF (D–F) or with R10B-lipoplex (G–I) in serum-free medium for 5 min and then stained with phalloidin-TRITC. Insets show images of boxed regions at 2× magnification. Arrows showed lamellipodia induced by EGF or R10B-lipoplex. Scale bar = 20 μm.

and KB cells. Macropinocytosis has the ability to avoid lysosomal degradation (Conner and Schmid, 2003; Medina-Kauwe et al., 2005; Meier et al., 2002); therefore, R10B-lipoplex might induce high gene expression in HeLa cells *via* macropinocytosis. DNA transfection efficiency with decaarginine-PEG-lipid was determined by cell line-dependent internalization pathways.

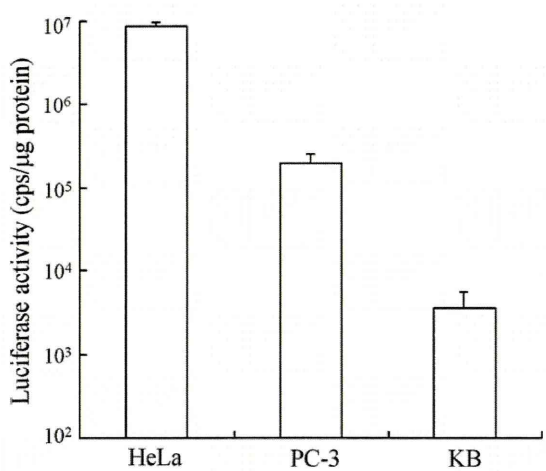

Fig. 6. Luciferase activities in HeLa (A), PC-3 (B) and KB cells (C) after transfection by R10B-lipoplex. The cells were incubated for 3 h in serum-free medium after transfection, and then incubated for another 21 h in medium containing 10% FBS. Each bar represents the mean ± S.D. of three experiments.

5. Conclusion

In this report, we demonstrated that the internalization of R10B-lipoplex occurred mainly through macropinocytosis in HeLa cells, and clathrin-mediated endocytosis in PC-3 and KB cells, not depending on HSPG amounts in each cell. Furthermore, R10B-lipoplex induced the highest gene expression in HeLa cells among their cell lines. Although the exact cellular uptake mechanism of R10B-lipoplex remains to be elucidated, the cellular uptake mechanism of the lipoplex might be dependent on the cell line and affect transfection activity.

Acknowledgements

This project was supported in part by a Grant-in-Aid for Scientific Research from the Ministry of Education, Culture, Sports, Science, and Technology of Japan, and by the Open Research Center Project.

References

Conner, S.D., Schmid, S.L., 2003. Regulated portals of entry into the cell. Nature 422, 37–44.

Console, S., Marty, C., Garcia-Echeverria, C., Schwendener, R., Ballmer-Hofer, K., 2003. Antennapedia and HIV transactivator of transcription (TAT) "protein transduction domains" promote endocytosis of high molecular weight cargo upon binding to cell surface glycosaminoglycans. J. Biol. Chem. 278, 35109–35114.

Derossi, D., Joliot, A.H., Chassaing, G., Prochiantz, A., 1994. The third helix of the Antennapedia homeodomain translocates through biological membranes. J. Biol. Chem. 269, 10444–10450.

Douglas, K.L., Piccirillo, C.A., Tabrizian, M., 2008. Cell line-dependent internalization pathways and intracellular trafficking determine transfection efficiency of nanoparticle vectors. Eur. J. Pharm. Biopharm. 68, 676–687.

Drin, G., Cottin, S., Blanc, E., Rees, A.R., Temsamani, J., 2003. Studies on the internalization mechanism of cationic cell-penetrating peptides. J. Biol. Chem. 278, 31192–31201.

Ferrari, A., Pellegrini, V., Arcangeli, C., Fittipaldi, A., Giacca, M., Beltram, F., 2003. Caveolae-mediated internalization of extracellular HIV-1 tat fusion proteins visualized in real time. Mol. Ther. 8, 284–294.

Fischer, R., Kohler, K., Fotin-Mleczek, M., Brock, R., 2004. A stepwise dissection of the intracellular fate of cationic cell-penetrating peptides. J. Biol. Chem. 279, 12625–12635.

Fuchs, S.M., Raines, R.T., 2004. Pathway for polyarginine entry into mammalian cells. Biochemistry 43, 2438–2444.

Fujiwara, T., Akita, H., Harashima, H., 2010. Intracellular fate of octaarginine-modified liposomes in polarized MDCK cells. Int. J. Pharm. 386, 122–130.

Furuhata, M., Danev, R., Nagayama, K., Yamada, Y., Kawakami, H., Toma, K., Hattori, Y., Maitani, Y., 2008. Decaarginine-PEG-artificial lipid/DNA complex for gene delivery: nanostructure and transfection efficiency. J. Nanosci. Nanotechnol. 8, 2308–2315.

Furuhata, M., Izumisawa, T., Kawakami, H., Toma, K., Hattori, Y., Maitani, Y., 2009. Decaarginine-PEG-liposome enhanced transfection efficiency and function of arginine length and PEG. Int. J. Pharm. 371, 40–46.

Furuhata, M., Kawakami, H., Toma, K., Hattori, Y., Maitani, Y., 2006a. Design, synthesis and gene delivery efficiency of novel oligo-arginine-linked PEG-lipids: effect of oligo-arginine length. Int. J. Pharm. 316, 109–116.

Furuhata, M., Kawakami, H., Toma, K., Hattori, Y., Maitani, Y., 2006b. Intracellular delivery of proteins in complexes with oligoarginine-modified liposomes and the effect of oligoarginine length. Bioconjug. Chem. 17, 935–942.

Futaki, S., Ohashi, W., Suzuki, T., Niwa, M., Tanaka, S., Ueda, K., Harashima, H., Sugiura, Y., 2001a. Stearylated arginine-rich peptides: a new class of transfection systems. Bioconjug. Chem. 12, 1005–1011.

Futaki, S., Suzuki, T., Ohashi, W., Yagami, T., Tanaka, S., Ueda, K., Sugiura, Y., 2001b. Arginine-rich peptides. An abundant source of membrane-permeable peptides having potential as carriers for intracellular protein delivery. J. Biol. Chem. 276, 5836–5840.

Grimmer, S., van, D.B., Sandvig, K., 2002. Membrane ruffling and macropinocytosis in A431 cells require cholesterol. J. Cell Sci. 115, 2953–2962.

Hattori, Y., Maitani, Y., 2007. DNA/Lipid complex incorporated with fibronectin to cell adhesion enhances transfection efficiency in prostate cancer cells and xenografts. Biol. Pharm. Bull. 30, 603–607.

Igarashi, S., Hattori, Y., Maitani, Y., 2006. Biosurfactant MEL-A enhances cellular association and gene transfection by cationic liposome. J. Control. Release 112, 362–368.

Jones, S.W., Christison, R., Bundell, K., Voyce, C.J., Brockbank, S.M., Newham, P., Lindsay, M.A., 2005. Characterisation of cell-penetrating peptide-mediated peptide delivery. Br. J. Pharmacol. 145, 1093–1102.

Kaplan, I.M., Wadia, J.S., Dowdy, S.F., 2005. Cationic TAT peptide transduction domain enters cells by macropinocytosis. J. Control. Release 102, 247–253.

Kawamura, K.S., Sung, M., Bolewska-Pedyczak, E., Gariepy, J., 2006. Probing the impact of valency on the routing of arginine-rich peptides into eukaryotic cells. Biochemistry 45, 1116–1127.

Khalil, I.A., Kogure, K., Futaki, S., Harashima, H., 2006. High density of octaarginine stimulates macropinocytosis leading to efficient intracellular trafficking for gene expression. J. Biol. Chem. 281, 3544–3551.

Kosuge, M., Takeuchi, T., Nakase, I., Jones, A.T., Futaki, S., 2008. Cellular internalization and distribution of arginine-rich peptides as a function of extracellular peptide concentration, serum, and plasma membrane associated proteoglycans. Bioconjug. Chem. 19, 656–664.

Medina-Kauwe, L.K., Xie, J., Hamm-Alvarez, S., 2005. Intracellular trafficking of non-viral vectors. Gene Ther. 12, 1734–1751.

Meier, O., Boucke, K., Hammer, S.V., Keller, S., Stidwill, R.P., Hemmi, S., Greber, U.F., 2002. Adenovirus triggers macropinocytosis and endosomal leakage together with its clathrin-mediated uptake. J. Cell Biol. 158, 1119–1131.

Mitchell, D.J., Kim, D.T., Steinman, L., Fathman, C.G., Rothbard, J.B., 2000. Polyarginine enters cells more efficiently than other polycationic homopolymers. J. Pept. Res. 56, 318–325.

Morris, M.C., Depollier, J., Mery, J., Heitz, F., Divita, G., 2001. A peptide carrier for the delivery of biologically active proteins into mammalian cells. Nat. Biotechnol. 19, 1173–1176.

Nakase, I., Niwa, M., Takeuchi, T., Sonomura, K., Kawabata, N., Koike, Y., Takehashi, M., Tanaka, S., Ueda, K., Simpson, J.C., Jones, A.T., Sugiura, Y., Futaki, S., 2004. Cellular uptake of arginine-rich peptides: roles for macropinocytosis and actin rearrangement. Mol. Ther. 10, 1011–1022.

Nakase, I., Tadokoro, A., Kawabata, N., Takeuchi, T., Katoh, H., Hiramoto, K., Negishi, M., Nomizu, M., Sugiura, Y., Futaki, S., 2007. Interaction of arginine-rich peptides with membrane-associated proteoglycans is crucial for induction of actin organization and macropinocytosis. Biochemistry 46, 492–501.

Nobes, C.D., Hall, A., 1995. Rho, rac, and cdc42 GTPases regulate the assembly of multimolecular focal complexes associated with actin stress fibers, lamellipodia, and filopodia. Cell 81, 53–62.

Oehlke, J., Scheller, A., Wiesner, B., Krause, E., Beyermann, M., Klauschenz, E., Melzig, M., Bienert, M., 1998. Cellular uptake of an alpha-helical amphipathic model peptide with the potential to deliver polar compounds into the cell interior non-endocytically. Biochim. Biophys. Acta 1414, 127–139.

Pooga, M., Hallbrink, M., Zorko, M., Langel, U., 1998. Cell penetration by transportan. FASEB J. 12, 67–77.

Potocky, T.B., Menon, A.K., Gellman, S.H., 2003. Cytoplasmic and nuclear delivery of a TAT-derived peptide and a beta-peptide after endocytic uptake into HeLa cells. J. Biol. Chem. 278, 50188–50194.

Rejman, J., Oberle, V., Zuhorn, I.S., Hoekstra, D., 2004. Size-dependent internalization of particles via the pathways of clathrin- and caveolae-mediated endocytosis. Biochem. J. 377, 159–169.

Richard, J.P., Melikov, K., Brooks, H., Prevot, P., Lebleu, B., Chernomordik, L.V., 2005. Cellular uptake of unconjugated TAT peptide involves clathrin-dependent endocytosis and heparan sulfate receptors. J. Biol. Chem. 280, 15300–15306.

Richard, J.P., Melikov, K., Vives, E., Ramos, C., Verbeure, B., Gait, M.J., Chernomordik, L.V., Lebleu, B., 2003. Cell-penetrating peptides. A reevaluation of the mechanism of cellular uptake. J. Biol. Chem. 278, 585–590.

Schlunck, G., Damke, H., Kiosses, W.B., Rusk, N., Symons, M.H., Waterman-Storer, C.M., Schmid, S.L., Schwartz, M.A., 2004. Modulation of Rac localization and function by dynamin. Mol. Biol. Cell 15, 256–267.

Suzuki, T., Futaki, S., Niwa, M., Tanaka, S., Ueda, K., Sugiura, Y., 2002. Possible existence of common internalization mechanisms among arginine-rich peptides. J. Biol. Chem. 277, 2437–2443.

Tyagi, M., Rusnati, M., Presta, M., Giacca, M., 2001. Internalization of HIV-1 tat requires cell surface heparan sulfate proteoglycans. J. Biol. Chem. 276, 3254–3261.

Vives, E., 2003. Cellular uptake of the Tat peptide: an endocytosis mechanism following ionic interactions. J. Mol. Recognit. 16, 265–271.

Vives, E., Brodin, P., Lebleu, B., 1997. A truncated HIV-1 Tat protein basic domain rapidly translocates through the plasma membrane and accumulates in the cell nucleus. J. Biol. Chem. 272, 16010–16017.

Wadia, J.S., Stan, R.V., Dowdy, S.F., 2004. Transducible TAT-HA fusogenic peptide enhances escape of TAT-fusion proteins after lipid raft macropinocytosis. Nat. Med. 10, 310–315.

Wender, P.A., Mitchell, D.J., Pattabiraman, K., Pelkey, E.T., Steinman, L., Rothbard, J.B., 2000. The design, synthesis, and evaluation of molecules that enable or enhance cellular uptake: peptoid molecular transporters. Proc. Natl. Acad. Sci. U.S.A. 97, 13003–13008.

Zaro, J.L., Shen, W.C., 2003. Quantitative comparison of membrane transduction and endocytosis of oligopeptides. Biochem. Biophys. Res. Commun. 307, 241–247.